Dynamical Properties of Ion-Acoustic Waves in Space Plasma and Its Application to Image Encryption

JHARNA TAMANG[1], **JEAN DE DIEU NKAPKOP**[2], **MUHAMMAD FAZAL IJAZ**[3],
PUNAM KUMARI PRASAD[1], **NESTOR TSAFACK**[4,5], **ASIT SAHA**[1],
JACQUES KENGNE[5], **AND YOUNGDOO SON**[6]

[1]Department of Mathematics, Sikkim Manipal Institute of Technology, Sikkim Manipal University, Majitar 737136, India
[2]Department of Electrical Engineering and Industrial Computing, University Institute of Technology, Douala, Cameroon
[3]Department of Intelligent Mechatronics Engineering, Sejong University, Seoul 05006, South Korea
[4]Research Unit of Laboratory of Condensed Matter, Electronics and Signal, Processing (URMACETS), Department of Physics, Faculty of Sciences, University of Dschang, Dschang, Cameroon
[5]Research Unit of Laboratory of Automation and Applied Computer (LAIA), Electrical Engineering Department, IUT-FV, University of Dschang, Bandjoun, Cameroon
[6]Department of Industrial and Systems Engineering, Dongguk University, Seoul 04620, South Korea

Corresponding authors: Muhammad Fazal Ijaz (fazal@sejong.ac.kr) and Youngdoo Son (youngdoo@dongguk.edu)

ABSTRACT The nonlinear ion-acoustic waves (IAWs) in a space plasma are capable of exhibiting chaotic dynamics which can be applied to cryptography. Dynamical properties of IAWs are examined using the direct method in plasmas composed of positive and negative ions and nonextensive distributed electrons. Applying the wave transformation, the governing equations are deduced into a dynamical system (DS). Supernonlinear and nonlinear periodic IAWs are presented through phase plane analysis. The analytical periodic wave solution for IAW is obtained. Under the influence of an external periodic force, the DS is transformed to a perturbed system. The perturbed DS describes multistability property of IAWs with change of initial conditions. The multistability behavior features coexisting trajectories such as, quasiperiodic, multiperiodic and chaotic trajectories of the perturbed DS. The chaotic feature in the perturbed DS is supported by Lyapunov exponents. This interesting behavior in the windows of chaotic dynamics is exploited to design efficient encryption algorithm. First SHA-512 is used to compute the hash digest of the plain image which is then used to update the initial seed of the chaotic IAWs system. Note that SHA-512 uses one-way function to map input data to the output, consequently it is quite impossible to break the proposed encryption technique. Second DNA coding is used to confuse and diffuse the DNA version of the plain image. The diffused image follows DNA decoding process leading to the cipher image. The security performance is evaluated using some well-known metrics and results indicate that the proposed cryptosystem can resist most of existing cryptanalysis techniques. In addition complexity analysis shows the possibility of practical implementation of the proposed algorithm.

INDEX TERMS Chaos, image encryption, ion-acoustic wave, multistability, periodic wave, superperiodic wave.

I. INTRODUCTION

The rapid development of the internet and the wide applications of multimedia technology have enable people to exchange information with high confidentiality [1], [2]. The security of data during its transmission involves several different aspects, including copyright protections, authentications, entertainments, business, health services and military affairs, etc. To fulfill a certain level of security in the wide range of applications, the encryption and decryption processes are very necessary. Some traditional or conventional encryption-decryption algorithms like DES (Data Encryption Standard), AES (Advanced Encryption Standard), IDEA (International Data Encryption Algorithm) and

The associate editor coordinating the review of this manuscript and approving it for publication was Naveed Akhtar.

RSA (developed by Rivest, Shamir and Adleman) have been used in the past in order to avoid malicious attacks from unauthorized parties [3], [4]. But it has been shown that these methods are inappropriate for digital image encryption-decryption due to some intrinsic properties of the images such as bulky data capacity and high redundancy, which are generally difficult to handle by using these traditional techniques [5], [6]. These conventional methods therefore are less useful in image encryption cryptography, especially for rapid communication applications. We can now realize that more and more research has been done to develop modern encryption algorithms [7]–[10]. For instance chaos based encryption are used to protect the transferred information from attacks [9]. Some researchers have been devoted to systems characterized by ergodicity, deterministic dynamics, unpredictable behavior, non-linear transform, sensitivity dependence on initial conditions and system's parameters. They used to investigate the dynamical properties of the proposed systems focusing on potential striking dynamical behavior including periodic attractors, chaotic attractors or hyperchaotic attractors, antimonotonicity, period doubling, crises, hysteresis, and coexisting bifurcations [11], [12]. Note that some of these properties and behaviors may be useful to image encryption in order to increase the number of encryption keys [7], [8].

Existing results in literature has recognized the presence of IAWs in plasmas comprising of negative and positive ions. The examination the negative ions in plasma system is significant owing to their broad applications in laboratory [13] and plasma processing reactors [14]. Saleem [15] presented the theoretical criterion for plasmas to have negative and positive ions. Many researchers [16]–[18], [20] reported the study of negative and positive pair ions for different plasma environments. Chaizy *et al.* [21] investigated that the negative ions in the comet Halley are readily damaged by solar radiation. The presence of negative ions is important in a physical processes such as radiative transfer or charge exchange that occur mainly in environments farther away from the Sun like Jupiter's or Saturn's magnetospheres. However, Coates *et al.* [22] recognized the presence of negative ions in Titan's atmosphere. These negative ions were considered to have high number densities and play a vital role in chemical process like formation of organic-rich aerosols.

The physical environments present on space and astrophysical systems such as, galaxy clusters [23], plasmas [24], contain high energy and long-range interaction particles. These particles form various classes of nonextensive systems and develop strong thermostatistics. The nonextensive entropy introduced by Tsallis [25] can be extensively used for particles with high energy. The entropy proposed for combined system $(X + Y)$ is explained by the relation, $S_q(X + Y) = S_q^{(X)} + S_q^{(Y)} + (1 - q)S_q^{(X)}S_q^{(Y)}$ where individually X and Y are two different systems. The measure of nonextensivity is expressed by q [26] and as $q \rightarrow 1$ the system becomes Maxwellian [27]. The experimental observation done by

Liu *et al.* [28] reported that the non-Gaussian statistics are framed by the Tsallis distribution. The Tsallis distribution function can be applied for a system which holds the relation $1 - q = dT/dE$, where E and T denote energy and temperature in energy units [29]. The relation [30] of q with potential energy and temperature gradient is given by $k\nabla T + (1 - q)m\nabla\phi = 0$. This stands for the reason that $q \neq 1$ as $\nabla T \neq 0$. This shows that q-nonextensive holds a physical significance to describe the velocity distribution occurring in various non-equilibrium stationary-state systems [31]. It is recorded that when $\nabla T = 0$ and $T = T_0$ =constant, $q \rightarrow 1$ that converges the nonextensive distribution to the Maxwellian one [31].

The nonlinear waves in multi-component plasmas are capable of generating interesting behaviors and one such feature is called supernonlinear waves discovered by Dubinov and Kolotkov [32], [33]. Such waves are classified by the number of singular points and sepratrix layers in their phase profiles. A nonlinear wave should at least three singular points and one sepratrix layer in order to be classified as supernonlinear waves. Recently, numerous works [34]–[36] were reported for studying supersolitons using the Sagdeev potential. Researchers also studied examined supernonlinear waves in three-component plasma model [37], [38] where two temperature electrons were considered. In four-component plasmas, very recently, El-Wakil *et al.* [39] reported the supernonlinear waves in non-Maxwellian plasmas. However, the studies of supernonlinear waves through the dynamical systems and phase plane analysis [40]–[42] have gathered great attention of researchers. It is interesting to know that many researchers have already studied nonlinear with different composition of plasma particles in different atmosphere [43]–[46]. The chaotic, periodic and quasiperiodic behaviors of dynamical systems in plasmas are reported in multi-constituent plasmas [47]. Rahim *et al.* [48] studied dynamical feature and multistability. Many researchers [49]–[52] reported multistability property that is widely used to examine dynamical features for various systems. Very recently, some studies [53]–[55] related to dynamical behavior and multistability property of nonlinear waves under different plasma compositions have been examined widely for various plasma atmospheres. In this study, we consider a plasma model [56] to study solitary, periodic and superperiodic waves and their multistability behavior. Furthermore, the considered plasma system supports chaotic dynamics of IAWs which is applied to image encryption.

It has been proved that chaotic sequences are useful for image encryption. Inverse tent map was used by T. Habutsu and co-workers to build a chaotic cryptosystem for image security [57], in which the initial states are calculated in terms of the original input image. The encrypted data is obtained for N iterations of the chaotic map. E. Biham presented a cryptanalysis based on weakness of the chaotic map (Ten maps) to break the above mentioned cryptosystem [58]. Using the sequence of the well-known one dimensional Logistic map,

M. S. Baptista designed an encryption scheme and security analysis indicated an efficient encryption process [59]. However most of the proposed algorithms rely on the solely use of chaotic sequences in the diffusion process. This may usually cause some lack of security and time consumption. Some solutions to these problems can be found in the literature. For instance, Wang and collaborators combined cyclic shift and sorting permutation technics to produce rapid image encryption protocol [9]. DNA can also be combined to chaotic sequences and other transformations to achieve more security and rapidity [60]. In this paper we combine the chaotic sequences of the proposed IAW with DNA coding and $SHA - 512$ to design a robust cryptosystem. First $SHA - 512$ is used to compute the hash digest of the plain image which is then used to update the initial seed of the chaotic IAW system. Second DNA coding is used to confuse and diffuse the DNA version of the plain image. The diffused image follows DNA decoding process leading to the cipher image.

The article is arranged as follows: In section II, mathematical model is considered. In section III, the dynamical system is formed using the direct method. In section IV, multistability properties are presented. In section V, encryption process and its security are discussed. In section VI, conclusion of our work is provided.

II. MODEL EQUATIONS

Supernonlinear and nonlinear IAWs are studied for a plasma system consisting of q-distributed electrons, negative and positive ions. The normalized governing equations [56] are:

$$\frac{\partial n_{p,n}}{\partial t} + \frac{\partial}{\partial x}(n_{p,n} u_{p,n}) = 0, \tag{1}$$

$$\frac{\partial u_p}{\partial t} + u_p \frac{\partial u_p}{\partial x} + \frac{\partial \phi}{\partial x} = 0, \tag{2}$$

$$\frac{\partial u_n}{\partial t} + u_n \frac{\partial u_n}{\partial x} - s \frac{\partial \phi}{\partial x} = 0, \tag{3}$$

$$\frac{\partial^2 \phi}{\partial x^2} - n_e - n_n + n_p = 0. \tag{4}$$

Here, n_e, n_n and n_p denote number densities of electron, negative and positive ions, respectively. These number densities are normalized by n_{p0}. Here, u_n and u_p are velocities normalized by $C_{si} = (T_e/m_p)^{1/2}$, ϕ denotes potential of electrostatic wave which is normalized by T_e/e. The time and space variables are t and x normalized by $\omega_{pp}^{-1} = (m_p/4\pi e^2 n_{p0})^{1/2}$ and $\lambda_{Dp} = (T_e/4\pi e^2 n_{p0})^{1/2}$, respectively. T_e represents electron temperature, e is electronic charge, $m_n(m_p)$ represents mass of negative (positive) ions and $s = m_p/m_n$. At equilibrium, we have $N_e = 1 - N_n$, where $N_e = n_{e0}/n_{p0}$ and $N_n = n_{n0}/n_{p0}$ are unperturbed number density ratios of electrons to positive ions and negative to positive ions, respectively.

The electron velocity distribution function

$$f_e(v) = C_q\{1 + (q-1)[\frac{m_e v^2}{2k_B T_e} - \frac{e\phi}{k_B T_e}]\}^{\frac{1}{(q-1)}},$$

with normalizing constant

$$C_q = n_{e0} \frac{\Gamma(\frac{1}{1-q})}{\Gamma(\frac{1}{1-q} - \frac{1}{2})} \sqrt{\frac{m_e(1-q)}{2\pi k_B T_e}} \text{ for } -1 < q < 1,$$

and

$$C_q = n_{e0} \frac{1+q}{2} \frac{\Gamma(\frac{1}{q-1} + \frac{1}{2})}{\Gamma(\frac{1}{q-1})} \sqrt{\frac{m_e(q-1)}{2\pi k_B T_e}} \text{ for } q > 1,$$

are considered to obtain the nonextensive number density of electrons. When $f_e(v)$ is integrated for all velocity spaces, one may obtain the following

$$n_e = n_{e0}\{1 + (q-1)\frac{e\phi}{k_B T_e}\}^{1/(q-1)+1/2},$$

where k_B is Boltzmann constant. After normalization, the number density of q-distributed electrons deduces to [61]

$$n_e = N_e\{1 + (q-1)\phi\}^{\frac{1}{q-1} + \frac{1}{2}}. \tag{5}$$

Here, q is nonextensive parameter with values higher than -1.

III. DYNAMICAL SYSTEM

The dynamical characteristics of IAWs are shown using tools such as, phase plane profiles, time series and Lyapunov exponents. In order to examine such diverse features of the wave, we transform the model equations into a planar dynamical system (DS) [41], [42] using the wave transformation $\xi = x - Vt$, where V is speed of the traveling wave. Substitution of ξ into equation (1) and integration w.r.t ξ applying conditions $n_p = 1$, $n_n = N_e$, $u_i = 0$, as $\xi \to \pm\infty$, the following relations are obtained

$$n_p = \frac{V}{V - u_p}, \quad n_n = \frac{VN_n}{V - u_n}. \tag{6}$$

Similarly, from equation (2) with conditions $u_n = 0$, $u_p = 0$, $\phi = 0$, as $\xi \to \pm\infty$, we get

$$V - u_p = \sqrt{V^2 - 2\phi}, \quad V - u_n = \sqrt{V^2 + 2s\phi}. \tag{7}$$

Solving equations (6) and (7), we obtain

$$n_p = \frac{V}{\sqrt{V^2 - 2\phi}}, \quad n_n = \frac{VN_n}{\sqrt{V^2 + 2s\phi}} \tag{8}$$

Substituting equations (4) and (8) in equation (3), we get

$$\frac{d^2\phi}{d\xi^2} - N_e[1 + (q-1)\phi]^{\frac{1}{q-1} + \frac{1}{2}} - \frac{VN_n}{\sqrt{V^2 + 2s\phi}} + \frac{V}{\sqrt{V^2 - 2\phi}} = 0. \tag{9}$$

We rewrite the above equation as

$$\frac{d^2\phi}{d\xi^2} = A\phi + B\phi^2 + C\phi^3, \tag{10}$$

where

$$A = \frac{1}{2}(1+q)N_e - \frac{sN_n}{V^2} - \frac{1}{V^2},$$

$$B = \frac{1}{8}(1+q)(3-q)N_e + \frac{3}{2V^4}s^2 N_n - \frac{3}{2V^4},$$

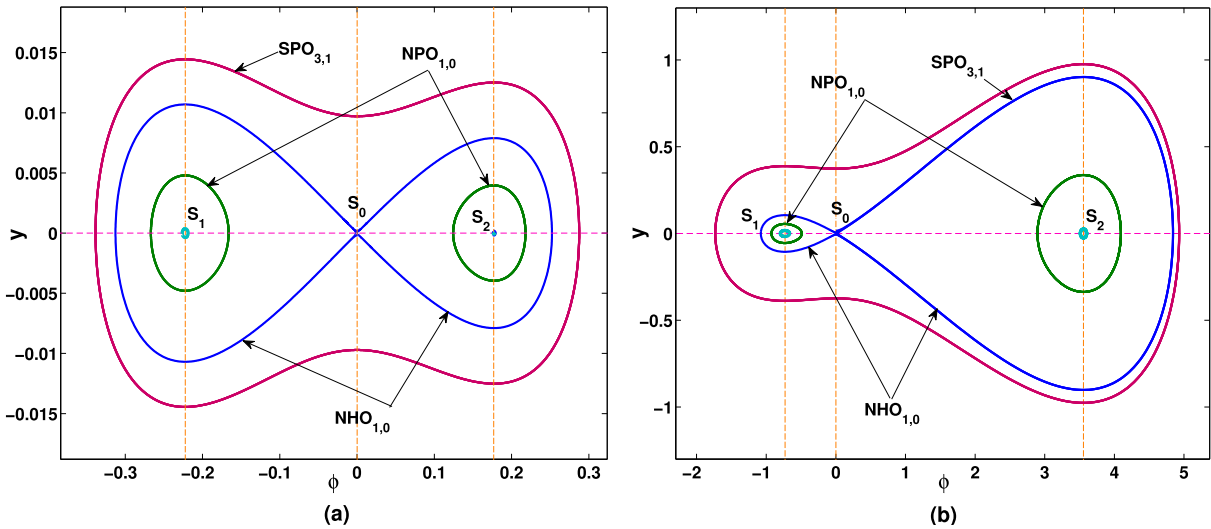$$C = \frac{1}{48}(1+q)(3-q)(5-3q)N_e - \frac{5}{2V^6}s^3 N_n - \frac{5}{2V^6}.$$

FIGURE 1. Phase portraits of system (11) for (a) $V = 1.4$, (b) $V = 1.47$ with $q = 0.4$, $n_{e0} = 1000$ cm^{-3}, $n_{n0} = 241.1$cm^{-3}, $m_p = 100$ amu, $m_n = 200$ amu.

The equation (10) is structured into the DS as follows

$$\begin{cases} \dfrac{d\phi}{d\xi} = z, \\ \dfrac{dz}{d\xi} = A\phi + B\phi^2 + C\phi^3. \end{cases} \quad (11)$$

For this study, we choose the Titan's atmosphere as our plasma environment. The Titan's atmosphere contains thin strata of methane and thicker strata of nitrogen. The observations of Cassini spacecraft revealed the existence of positive ions on the ionosphere of the Titan. Coates *et al.* [22] examined the presence of heavy negative ions in upper layer of the Titan's ionosphere. The negative ions consist of number density 100 cm^3, and masses of 10-30, 30-50, 50-80, 80-110, 110-200 and 200+ amu/charge. The ions with negative charge causes the electrostatic disturbances traveling in the atmosphere. The parameter q in superextensive case is restricted to $1/3 < q < 1$ [62]–[64]. Therefore, we consider the acceptable ranges $1/3 < q < 1$ and $q > 1$, and other plasma parameters from the data values of Titan's atmosphere [22], [56].

Figure 1 is phase portraits for the system DS (11) with higher unperturbed number density of negative ions $n_{n0} = 241.1$cm^{-3} with (a) $V = 1.4$, (b) $V = 1.47$ and $q = 0.4$, $n_{e0} = 1000$ cm^{-3}, $m_p = 100$ amu, $m_n = 200$ amu for superextensive case ($1/3 < q < 1$). Figure 1 contains three singular points S_0, S_1 and S_2 where S_0 is a saddle and S_1, S_2 are centers. Here, we observe that there exists three different families of orbits, namely, the nonlinear periodic orbit (NPO$_{1,0}$), nonlinear homoclinic orbit (NHO$_{1,0}$) and supernonlinear periodic orbit (SPO$_{3,1}$). Here, NPO$_{1,0}$ and NHO$_{1,0}$ enclose one singular point and contain no separatrix. However, SPO$_{3,1}$ contains three singular points and one separatrix. Every orbits in phase profiles of the dynamical system are related to wave solutions. Therefore, the NPO$_{1,0}$, NHO$_{1,0}$ and SPO$_{3,1}$ are associated to nonlinear periodic IAW (NPIAW) and nonlinear ion-acoustic solitary wave (NIASW) and supernonlinear periodic ion-acoustic wave (SPIAW) solutions.

Figure 2 is phase portraits for the system DS (11) with lower unperturbed number density of negative ions $n_{n0} = 8.99$cm^{-3} with (a) $q = 1.2$ and (b) $q = 2.2$, and $n_{e0} = 1000$cm^{-3}, $m_p = 100$ amu, $m_n = 200$ amu and $V = 0.9$ in subextensive case ($q > 1$). Figure 2 contains three singular points S_0, S_1 and S_2 where S_0 is a center in figure 2 (a) and S_0 is a saddle in figure 2 (b). This change is observed by changing the value of nonextensive parameter q and keeping all other parameters fixed. Here, we observe that there exists NPO$_{1,0}$, NHO$_{1,0}$ and SPO$_{3,1}$). Here, NPO$_{1,0}$ and NHO$_{1,0}$ enclose one singular point and contain no separatrix. Therefore, we observe the existence of NPIAW, NIASW and SPIAW for corresponding orbits, NPO$_{1,0}$, NHO$_{1,0}$ and SPO$_{3,1}$.

Figure 3 shows phase portraits of the system DS (11) for (a) superextensive case ($q = 0.5$), $V = 1.51$ and higher unperturbed number density of negative ions $n_{n0} = 241.1$cm^{-3} and (b) subextensive case ($q = 6$), $V = 0.9$ and lower unperturbed number density of negative ions $n_{n0} = 8.99$cm^{-3} with $n_{e0} = 1000$cm^{-3}, $m_p = 100$ amu, $m_n = 200$ amu and $V = 0.9$. Here, we observe from figure 3 that phase portrait of DS (11) contains three singular points S_0, S_1 and S_2 where $(0, 0)$ is a saddle. There exist NPO$_{1,0}$ and NHO$_{1,0}$ which encloses one singular point with no separatrix and, there is no sign of an orbit that encloses three singular points with at least one separatrix. Therefore, there exist no superperiodic feature for the above set of data values. This shows that supernonlinear feature is not supported for all the data values of the plasma systems.

A. WAVE SOLUTIONS FOR IAW

We encounter the existence of nonlinear periodic, nonlinear solitary and superperiodic solutions of IAWs through the
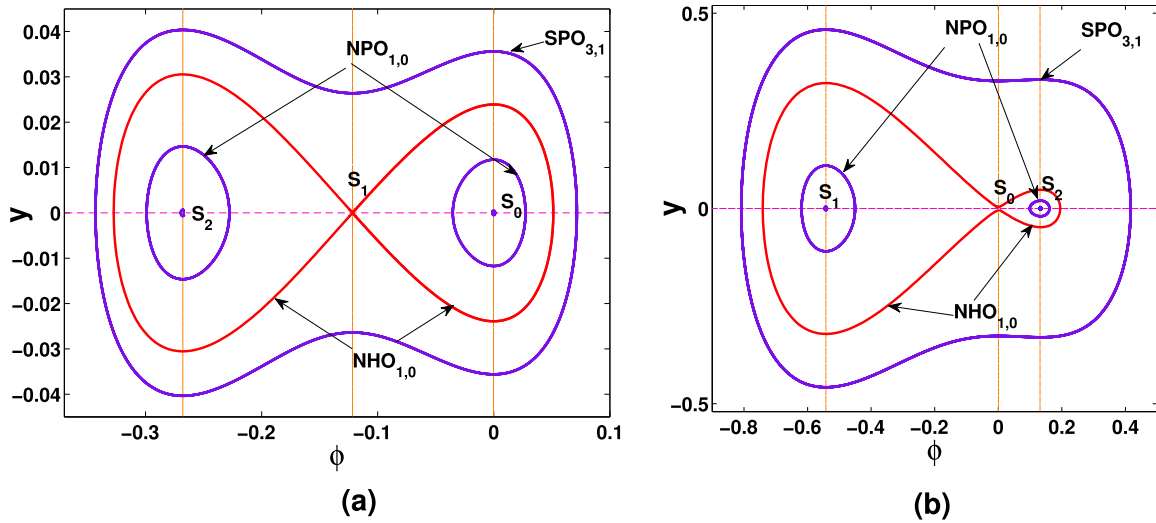
FIGURE 2. Phase portraits of system (11) for (a) $q = 1.2$ and (b) $q = 2.2$ with $n_{n0} = 8.99 \text{cm}^{-3}$, $n_{e0} = 1000 \text{cm}^{-3}$, $m_p = 100$ amu, $m_n = 200$ amu and $V = 0.9$.
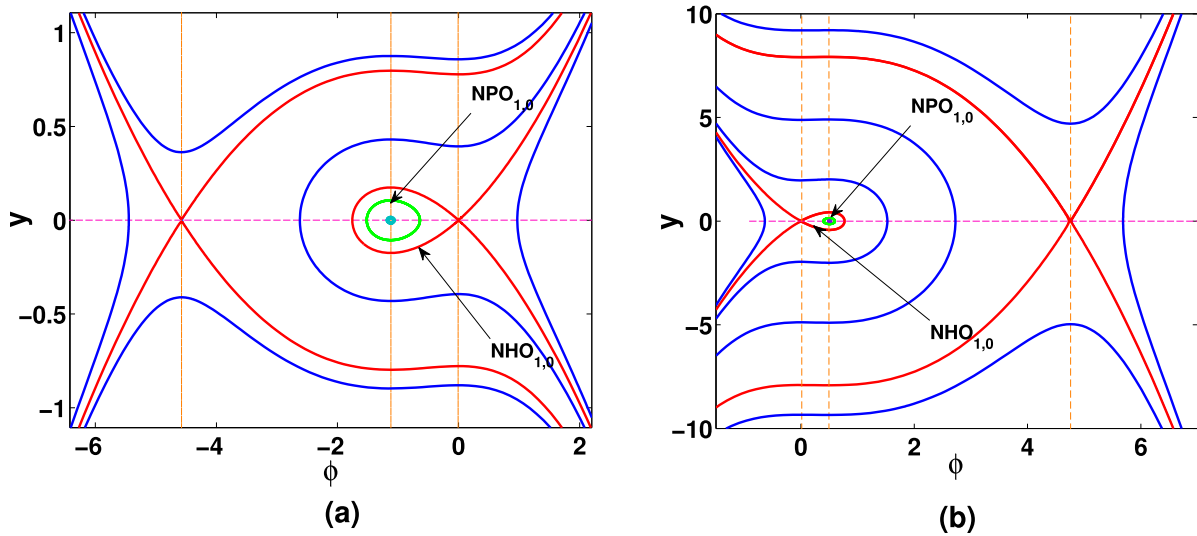

FIGURE 3. Phase portraits of system (11) for (a) $q = 0.5$, $V = 1.51$, $n_{n0} = 241.1 \text{cm}^{-3}$ and (b) $q = 6$, $V = 0.9$, $n_{n0} = 8.99 \text{cm}^{-3}$ with $n_{e0} = 1000 \text{cm}^{-3}$, $m_p = 100$amu, $m_n = 200$ amu.

phase plane analysis. Therefore, we now obtain the analytical periodic wave solution of IAW for which we suppose the Hamiltonian function $H(\phi, 0)$ of the DS (11) for which we get

$$H(\phi, y) = \frac{y^2}{2} - \left(\frac{A\phi^2}{2} + \frac{B\phi^3}{3} + \frac{C\phi^4}{4} \right) = h. \quad (12)$$

After simplification, we get

$$\frac{d\phi}{d\xi} = \sqrt{\frac{C}{2}} \sqrt{(a - \phi)(\phi - b)(\phi - c)(\phi - d)}, \quad (13)$$

where a, b, c and d are roots of $h_i + \frac{C}{2} \left(\phi^4 + \frac{4B}{C}\phi^3 + \frac{2A}{C}\phi^3 \right) = 0$.

Substituting equation (13) in (12), we get

$$\phi = \frac{b - c \left\{ \dfrac{a - b}{a - c} sn^2 \left(\dfrac{1}{g}\sqrt{\dfrac{C}{2}}\xi, k \right) \right\}}{1 - \dfrac{a - b}{a - c} sn^2 \left(\dfrac{1}{g}\sqrt{\dfrac{C}{2}}\xi, k \right)}. \quad (14)$$

The solution (14) is the analytical nonlinear periodic solution of IAW, where sn is the Jacobi elliptic function [65], $g = \dfrac{2}{\sqrt{(a - c)(b - d)}}$ and $k = \sqrt{\dfrac{(a - b)(c - d)}{(a - c)(b - d)}}$. The nonlinear solitary and periodic wave solutions are reported in [66], [67] and supernonlinear periodic in [68]. Now, we examine the changes caused by the variations of nonextensive parameter q and wave speed V on numerically obtained NPIAW and SPIAW for the considered plasma system.
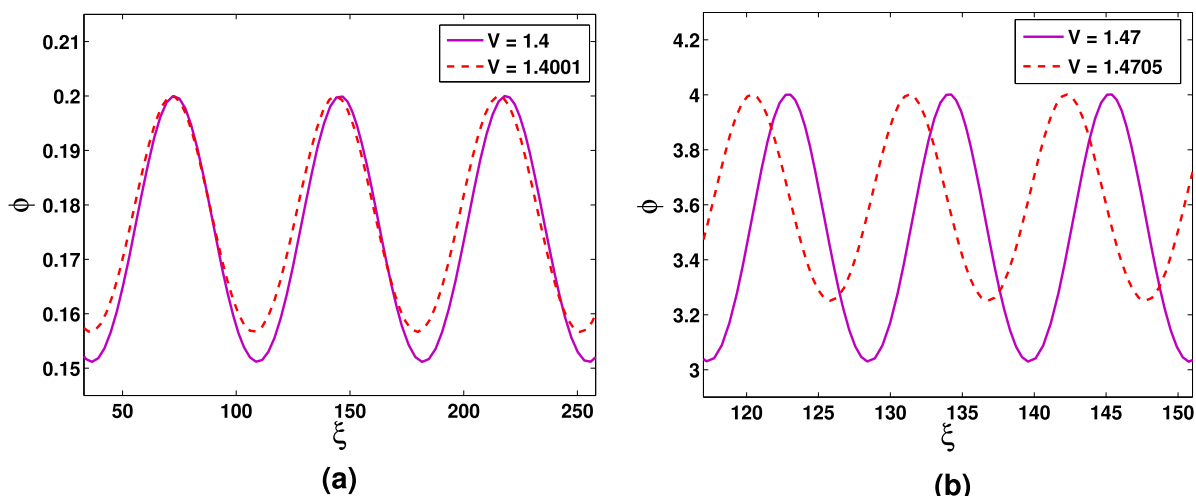
FIGURE 4. Periodic solution with respect to figure 1 (a) and (b) for different values of V.
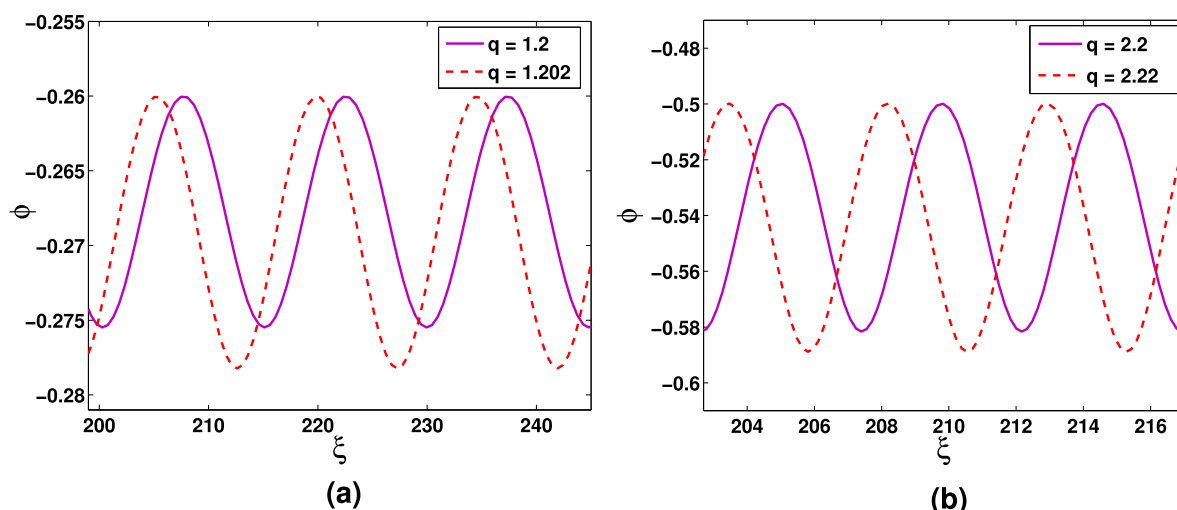

FIGURE 5. Periodic solution with respect to figure 2 (a) and (b) for different values of q.

Figure 4 displays change on NPIAW by varying V in the superextensive case ($1/3 < q < 1$) and keeping other values fixed as figure 1. As observed from figure 4 (a), as speed of wave (V) is slightly increased then amplitude of NPIAW gradually decreases. From figure 4 (b), we observe that amplitude of NPIAW decreases significantly as V tends to infinity. Therefore, we perceive that with higher values of V, the NPIAW becomes smooth.

Figure 4 shows change on NPIAW by varying q in the subextensive case $q > 1$ with keeping other values fixed as figure 1. As observed from figures 5 (a) and (b), when values of nonextensive parameter grows, amplitude of NPIAW rises. Therefore, for $q \rightarrow \infty$, we observe that the NPIAW becomes spiky.

Figure 6 shows change on SPIAW by varying q in the superextensive case ($1/3 < q < 1$) and keeping other values fixed as figure 1. From figure 6 (a), it is seen that for higher

values of wave speed (V), the amplitude of SPIAWs slightly decreases and its wideness grows resulting into smoothing of SPIAWs. From figure 6 (b), we observe that the amplitude of SPIAWs rises smoothly while its wideness shrinks making the SPIAW spiky for $V \rightarrow \infty$.

Figure 7 shows change on SPIAW by varying q in the subextensive case $q > 1$ and keeping other values fixed as figure 2. From figure 7 (a) and (b), we observe that for higher values of nonextensive parameter q, the amplitude of SPIAWs significantly extends while its wideness shrinks gradually. Thus, the SPIAW becomes spiky for $q \rightarrow \infty$.

IV. MULTISTABILITY PROPERTY
The dynamical features such as, chaotic and quasiperiodic behaviors of the system (11) are studied by introducing an extraneous force $f_0 \, cos(\omega \xi)$ in the system (11). To study coexisting trajectories or multistability features [11], [12] of
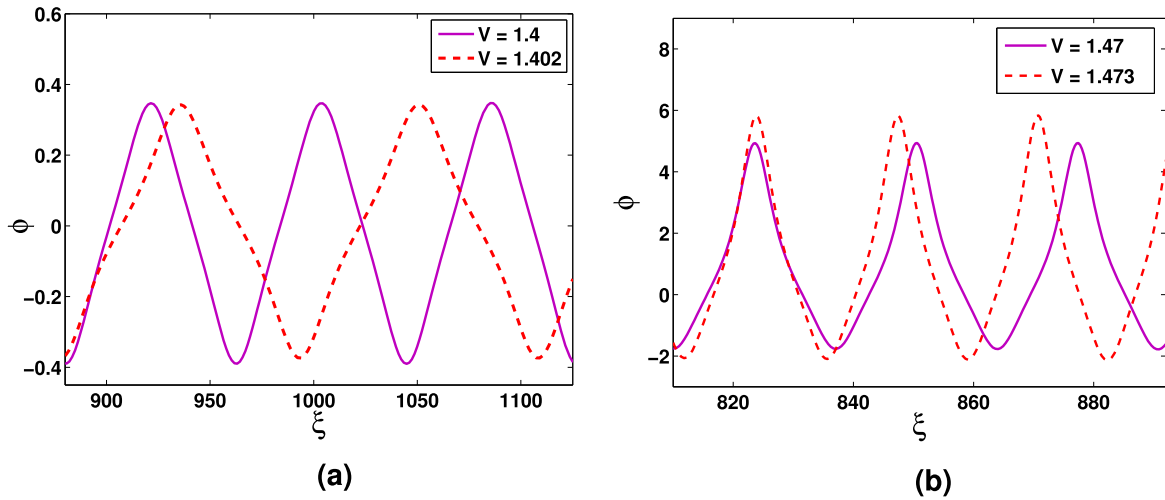
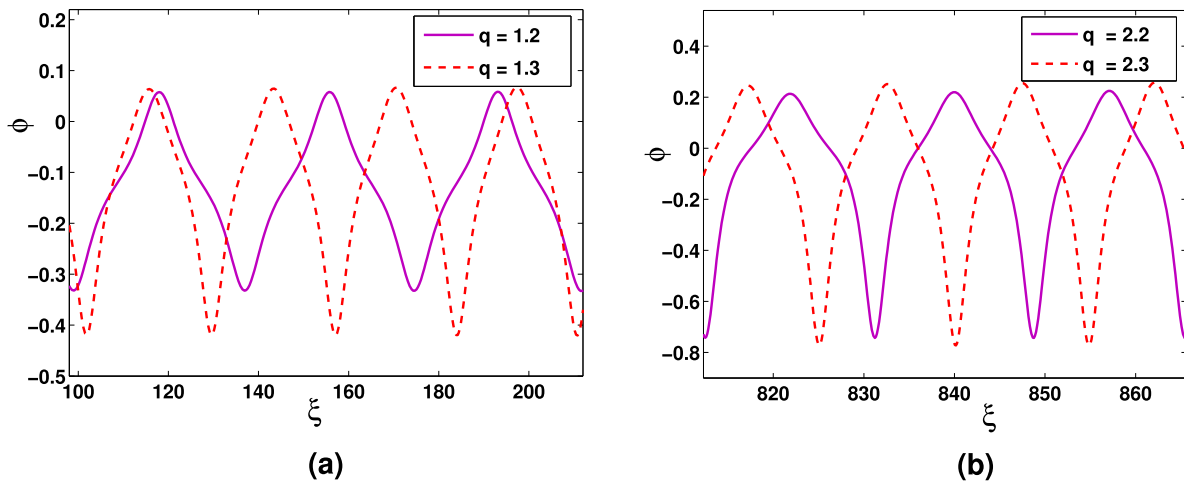**FIGURE 6.** Superperiodic solution with respect to figure 1 (a) and (b) for different values of V.

FIGURE 7. Superperiodic solution with respect to figure 2 (a) and (b) for different values of q.

a system (15), it is necessary to disturb the initial conditions $(\phi_0, y_0, 0)$ under the constant values of system parameters. Then, we obtain the perturbed dynamical system as,

$$\begin{cases} \dfrac{d\phi}{d\xi} = y, \\ \dfrac{dy}{d\xi} = A\phi + B\phi^2 + C\phi^3 + f_0 \, cos(U), \\ \dfrac{dU}{d\xi} = \omega, \end{cases} \quad (15)$$

where $U = \omega\xi$, f_0 is frequency and ω is strength of an external force [69], [70]. The perturbed system behaves differently under extraneous periodic force. Such system exhibits randomness and irregularity of trajectories. In our study, such trajectories show chaotic motions. The multistability feature [71]–[73] is exhibited by a perturbed DS when there exist two or more dynamic properties such as chaos, quasiperiodic, periodic and multiperiodicity for same set of parameters but distinct initial conditions.

Figure 8 shows phase portraits for system (15) in $\phi - y$ plane which reveal the existence of different coexisting orbits for both subextensive ($q > 1$) and superextensive ($q < 1$) cases. In figure 8 (*a*), we set $y_0 = 0.601$ with the system parameters $q = 2.2$, $n_{e0} = 1000 \text{ cm}^{-3}$, $n_{n0} = 8.99 \text{ cm}^{-3}$, $m_p = 100 \text{ amu}$, $m_n = 200 \text{ amu}$, $V = 0.9$, $f_0 = 1.9$, $\omega = 2.8$ and vary ϕ_0 of the initial condition. In this case, a chaotic orbit and two different types of multi-periodic orbits are obtained for $\phi_0 = 0.401$, $\phi_0 = 0.0401$ and $\phi_0 = -0.08$, respectively. When $f_0 = 0.09$ and other parameters same as in figure 8 (*a*) with $y_0 = 0.061$ of initial condition, we get figure 8 (*a*) which exhibit a single-periodic and three distinct quasiperiodic orbits for $\phi_0 = 0.202$, $\phi_0 = 0.201$, $\phi_0 = -0.094$ and $\phi_0 = -0.092$, respectively. In figure 8 (*c*), we fix $\phi_0 = -0.0524$ and fluctuate the y coordinate of the initial condition to demonstrate the coexistence of a multi-periodic and two different quasiperiodic orbits for $q = 0.4$, $n_{e0} = 1000 \text{ cm}^{-3}$, $n_{n0} = 8.99 \text{ cm}^{-3}$, $m_p = 100 \text{ amu}$, $m_n = 200 \text{ amu}$, $V = 0.94$, $f_0 = 0.6$, $\omega = 0.58$. The multiperiodic orbit colored in
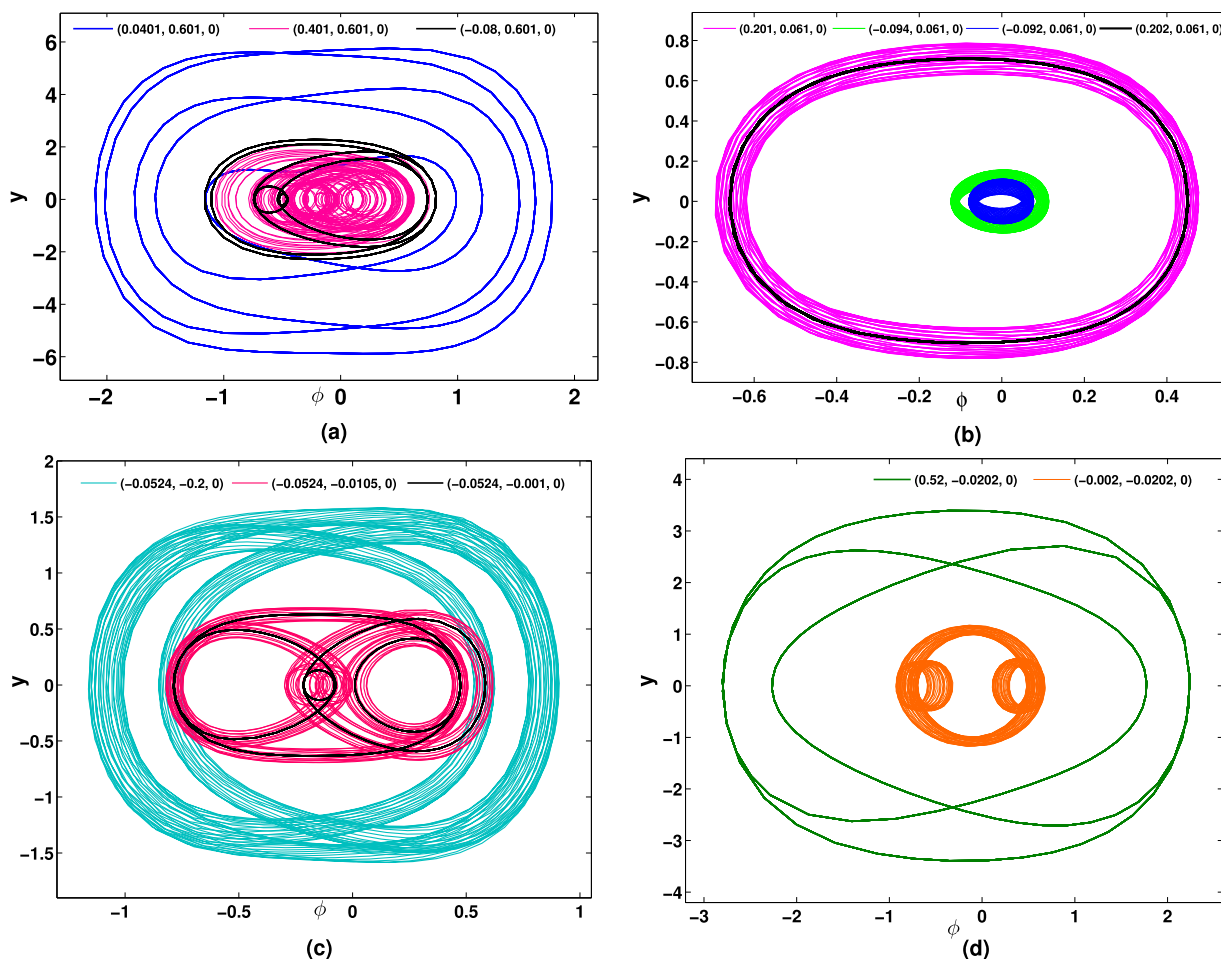
FIGURE 8. Multistability of system (15) for (a) subextensive case with $V = 0.9$, $f_0 = 1.9$, $\omega = 2.8$ (b) subextensive case with $V = 0.9$, $f_0 = 0.09$, $\omega = 2.8$ (c) superextensive case with $V = 0.94$, $f_0 = 0.6$, $\omega = 0.58$, and (d) superextensive case with $V = 1.4$, $f_0 = 1.16$, $\omega = 2.03$.

black exists for $y_0 = -0.001$, quasiperiodic orbits colored in red and ocean blue are obtained for $y_0 = -0.0105$ and $y_0 = -0.2$, respectively. Figure 8 (*c*) is acquired when $V = 1.4$, $f_0 = 1.16$, $\omega = 2.03$ and other parameters as figure 8 (*c*). Here, the system is shown to supports a quasiperiodic and a multiperiodic orbits for initial condition $(-0.002, -0.0202, 0)$ and $(0.52, -0.0202, 0)$, respectively. Figure 9 (a) and (b) shows time series plots corresponding to the multistability behaviors presented in figure 8(a) and (b) for subextensive region and lower number density of negative ions. Figure 9 (c) and (d) presents time series plots corresponding to the multistability behaviors presented in figure 8(c) and (d) for superextensive region and higher number density of negative ions.

The Lyapunov exponent is an efficient tool to determine the chaotic behavior of a system. Positive values of Lyapunov exponent show occurrence of chaos. Since, we observed the existence of chaos in multistability phase plot figure 8 (a) for the perturbed system (15), we determine the Lyapunov exponent with respect to f_0. From figure 10 we observe positive values of Lyapunov exponent that show occurrence of chaotic behavior in perturbed (15) corresponding to figure 8 (a). The intense chaotic feature is observed at $f_0 = 1.934$.

V. ENCRYPTION APPLICATION
A. PROPOSED ALGORITHM
1) SHA-512 FOR CRYPTOGRAPHY
Secure Hash Algorithm 512 (SHA−512) is one of the prominent solutions to withstand various forms of attacks in cryptography given than it is not reversible [74]. In effect SHA-512 accept any type of input data of any size and provide an output (hash digest) of 512 bits. Note that SHA-512 uses one-way function to map input data to the output, in addition a slight change in the input data leads to a completely different output. Consequently it is quite impossible to break encryption schemes based on SHA-512.

2) DNA PRINCIPLE FOR CRYPTOGRAPHY
Due to low power consumption and large memory capacity DNA coding has been shown to be efficient to cryptography in general and particularly in image encryption. It is well known that the four bases of DNA sequence are Adenine (A), Thymine (T), Guanine (G) and Cytosine (C) where A-T are complementary and C-G are complementary. Comparing to the binary system where 0 and 1 are complementary a correspondence can be defined as $00 \rightarrow A$, $11 \rightarrow T$,
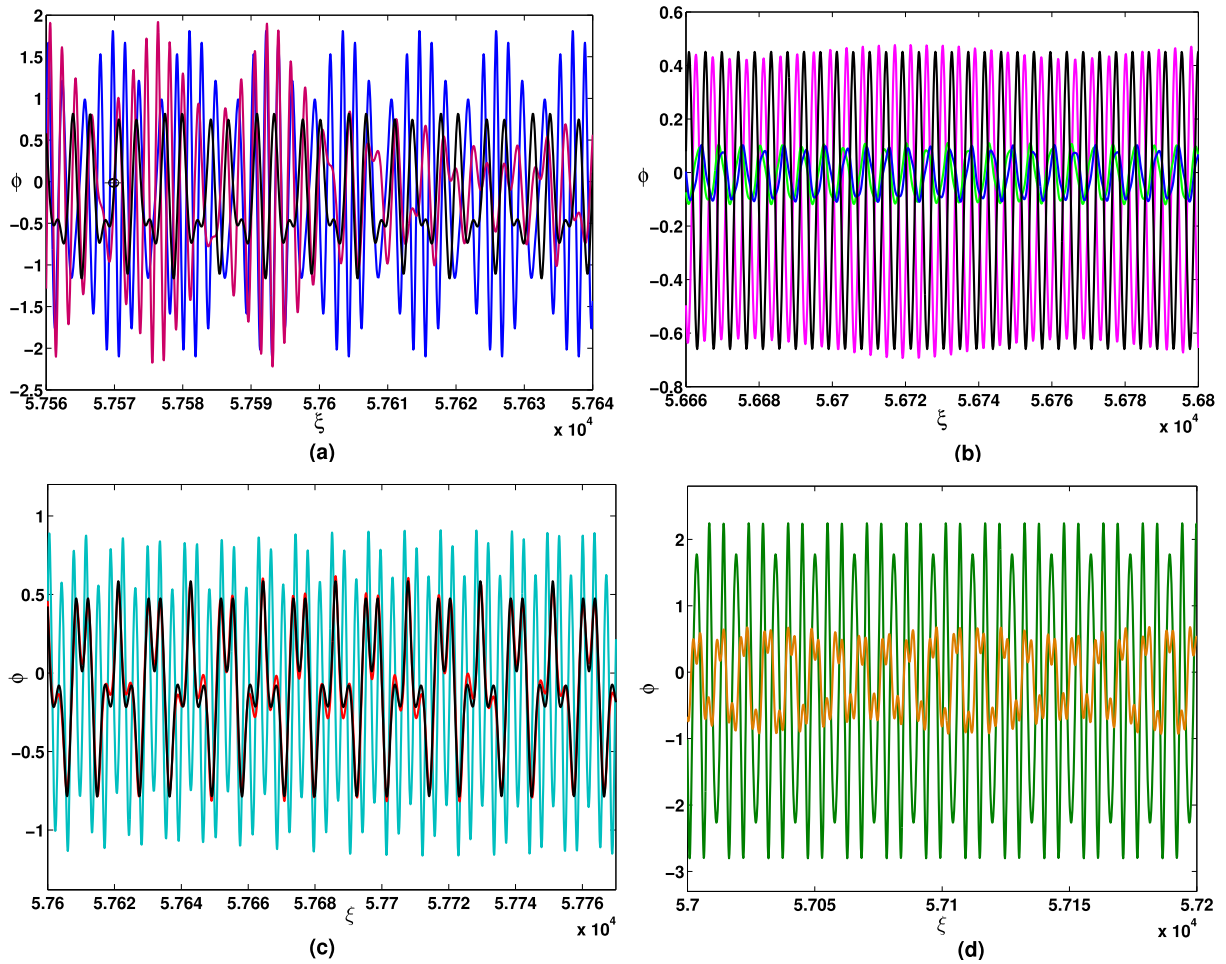
FIGURE 9. Time series plots corresponding to multistability behaviors of system (15) for (a) and (b) subextensive case and, (c) and (d) superextensive case shown in figure 8.
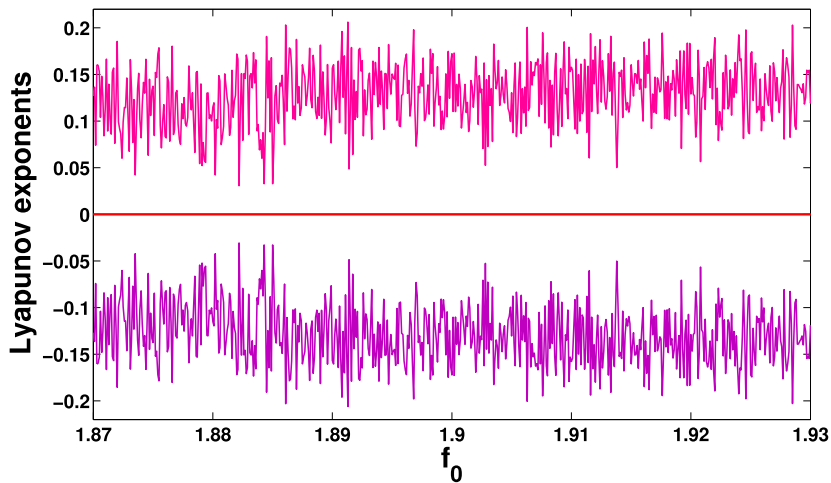
FIGURE 10. Lyapunov exponent for the chaotic behavior (shown by pink orbits in figure 8 (a)) of the perturbed DS (15) for subextensive case.

$01 \rightarrow C$, $10 \rightarrow D$. Some DNA operations like addition (*add*), subtraction (*sub*), multiplication (*mult*), exclusive-or (*ex_or*) and exclusive-nor (*ex_nor*) (Tables shown in FIGURE 11) are commonly used to enhance the diffusion process in encryption algorithms.

3) THE ENCRYPTION PROCESS

We start the encryption process by applying NIST SP 800-22 tests to the chaotic sequences to assess its randomness. The results in TABLE 2 indicate that the generated sequences (ϕ_i, y_i, u_i) are sufficiently random to find application in

add	A	C	G	T		sub	A	C	G	T		mult	A	C	G	T
A	C	A	T	G		A	C	G	T	A		A	T	G	C	A
C	A	C	G	T		C	A	C	G	T		C	G	T	A	C
G	T	G	C	A		G	T	A	C	G		G	C	A	T	G
T	G	T	A	C		T	G	T	A	C		T	A	C	G	T

ex_or	A	C	G	T		ex_nor	A	C	G	T
A	A	C	G	T		A	T	G	C	A
C	C	A	T	G		C	G	T	A	C
G	G	T	A	C		G	C	A	T	G
T	T	G	C	A		T	A	C	G	T

FIGURE 11. Some DNA operations.

cryptography that is p-values < 0.025 or p-values > 0.975. An encryption scheme based on the sequence of the proposed chaotic system with SHA-512 algorithm and DNA sequences is designed. The general outline of the whole encryption process is provided in Figure 12 and is described as follows:

Step 1: Read the plain image P_1 of size $m \times n \times r$ and compute its hash digest $H = H_1, H_2 \cdots H_{64}$ using SHA-512 where H_i is the ith byte in the digest H.

Step 2: Read the initial values ϕ_0, y_0, u_0 and apply the following update law for solving system (15):

$$\widetilde{\phi} = \left[\phi(0) + \frac{1}{10^{15}} \prod_{i=1}^{16} bin2dec(H_i)\right] mod\, 256$$

$$\widetilde{y} = \left[y(0) + \frac{1}{10^{15}} \prod_{i=17}^{32} bin2dec(H_i)\right] mod\, 256$$

$$\widetilde{u} = \left[u(0) + \frac{1}{10^{15}} \prod_{i=33}^{48} bin2dec(H_i)\right] mod\, 256 \qquad (16)$$

where $bin2dec$ converts the binary values of the hash digest to equivalent decimal values.

Step 3: Using the updated initial values, solve system (15) to obtain three chaotic sequences ϕ_i, y_i, u_i each of size $m \times n \times r$, convert each sequence into integers then into binary format.

Step 4: Apply DNA coding operation on the plain image P_1 using ϕ_i as indicated by TABLE 1 to achieve DNA matrix P_2.

Step 5: Apply DNA permutation operation on the DNA matrix P_2 following algorithm 1 to achieve the permuted matrix P_3.

Step 6: Apply DNA diffusion operation on the permuted matrix P_3 following algorithm 2 to achieve the diffused matrix P_4.

Step 7: Apply DNA decoding operation on the diffused matrix P_4 following the rules of TABLE 1.

B. SECURITY PERFORMANCE

To test and evaluate the security of the above cryptosystem, the proposed chaotic system is solved with initial seed as: $\widetilde{\phi} = -0.0524; \widetilde{y} = -0.2; \widetilde{u} = 0$; and system parameter as $A = 0.4490; B = -1.5998; C = -3.7125; f_0 = 1.9$. The data set is composed of two gray scale images and two color images each of size 256×256. All the simulations were carried on a workstation equipped with Intel core TM
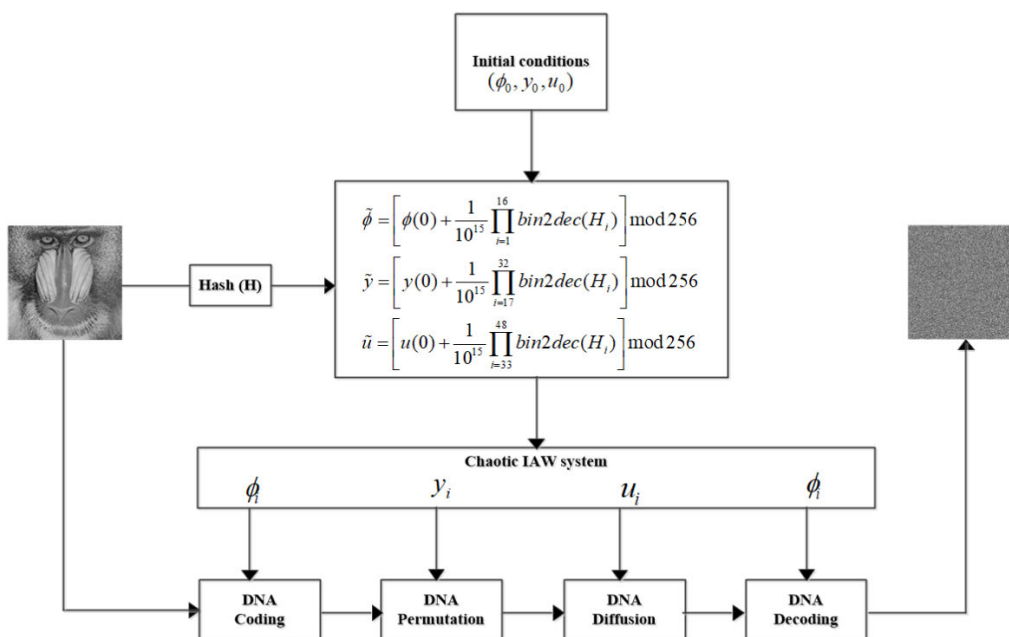

FIGURE 12. General outline of the encryption process. The decryption is reverse of the encryption process.

Algorithm 1: DNA Permutation Algorithm

Input: - P_2 is the DNA image obtained from DNA coding,
-[m,n,r] is the size of the DNA image.
-y is a chaotic sequence from system (15).

Output: Permuted matrix P_3.

Convert the chaotic sequence y into integers of range from 1 to m using $Y_{Int} = fix(y \times 10^{14} mod\ m) + 1$;

Collect the first different m elements from Y_{Int} sequence as (F); Permute the DNA image P_2 using permutation sequence F as:

for $i = 1 : m$ **do**
  for $j = 1 : n$ **do**
    for $k = 1 : r$ **do**
      $P_3(i, j, k) = P_2(F(i), F(j), k)$
    end
  end
end

---

i7-3630QM 16 GB RAM and MATLAB R2014b software. With reference to the results of Figure 13, the test images are visually unidentifiable. The PSNR of the encrypted image is computed with reference to the original image using the following formula:

$$PSNR = \log \frac{peak\_value}{MSE} \qquad (17)$$

where $peak\_value = 255$ for 8-bits images and MSE is the mean squared error computed as:

$$MSE = -\frac{1}{m \times n} \sum_{i=1}^{m} \sum_{j=1}^{n} [P(i,j) - C(i,j)]^2 \qquad (18)$$

where P and C are the plain and encrypted images of size $m \times n$ respectively. We achieved very low values of PSNR indicating that human eyes can not retrieve any significant information from the cipher image. However, few security analysis techniques such as, differential and statistical analyses are required to be performed to verify the encryption process.

1) CORRELATION OF ADJACENT PIXELS

The calculation of the correlation coefficient between the pixels makes it possible to evaluate the cryptographic quality of the cryptosystem. The correlation coefficient tends to 1 or -1 for two pixels that are closely associated. However, its value close to zero signs that the two pixels are not associated and cannot be predicted [75]. This metric is calculated from the following formula:

$$r_{xy} = \frac{E((x - E(x))(y - E(y)))}{\sqrt{D(x)}\sqrt{D(y)}},$$

where $E(x) = \frac{1}{N} \sum_{i=1}^{N} x_i$ and $D(x) = \frac{1}{N} \sum_{i=1}^{N} (x_i - E(x))^2$.

$$(19)$$

Algorithm 2: DNA Diffusion Algorithm

Input : - P3 is the DNA permuted image,
-[m,n,r] is the size of the DNA image.
-u is a chaotic sequence from system (15).

Output: Diffused matrix P_4.

Convert the chaotic sequence u into integers of range from 1 to n using $U_{Int} = fix(u \times 10^{14}\ mod\ m) + 1$;

Collect the first different $m \star n \star r$ elements from U_{Int} sequence as (L);

Construct the DNA diffusion key *Diff* as:

for $i = 1 : m \times n \times r$ **do**
  if *(L(i)==1 or L(i)==2)* **then**
    {Diff(i)=A}:
    else if *(L(i)==3 or L(i)==4)* **then**
      {Diff(i)=T}
    else if *(L(i)==5 or L(i)==6)* **then**
      {Diff(i)=C}
    else
      {Diff(i)=G}
  end
end

add, sub, ex_or, ex_nor and mult are different DNA operation as indicated in Figure 11.

Diffuse the DNA permuted image P3 using DNA diffusion key Diff as:

for $i = 1 : m \times n \times r$ **do**
  if *(L(i)==1)* **then**
    {P_4(i)=add(P_3(i), Diff(i))}:
    else if *(L(i)==2)* **then**
      {P_4(i)=sub(P_3(i), Diff(i))}
    else if *(L(i)==3)* **then**
      {P_4(i)=ex_or(P_3(i), Diff(i))}
    else if *(L(i)==4)* **then**
      {P_4(i)=ex_nor(P_3(i), Diff(i))}
    else
      {P_4(i)=mult(P_3(i),Diff(i))}
  end
end

TABLE 1. DNA coding and decoding rules.

Rules	Rule 1	Rule 2	Rule 3	Rule 4	Rule 5	Rule 6	Rule 7	Rule 8
00	A	A	C	C	G	G	T	T
01	C	G	A	T	A	T	C	G
10	G	C	T	A	T	A	G	C
11	T	T	G	G	C	C	A	A

Here x and y are the values of the gray level of the pixels at the same index of the images I and I', $E(x)$ and $D(x)$ are the variances with the number (N) of used pixels. TABLE 3 groups together the correlation coefficients obtained from the original and encrypted gray scale images and TABLE 4 groups together the correlation coefficients achieved from the original and encrypted color images. It appears that the

TABLE 2. Outcome of NIST SP 800-22 tests.

Statistical test	P-Value			Result
	$\phi_i\_p-values$	$y_i\_p-values$	$u_i\_p-values$	
Overlapping templates	0.407271	0.650450	0.359120	Passed
DFT	0.152887	0.781109	0.860403	Passed
Serial 1	0.717756	0.754489	0.125148	Passed
Serial 2	0.103093	0.585427	0.815041	Passed
Non overlapping templates	0.275189	0536478	0.125478	Passed
Frequency	0.833668	0.179596	0.431867	Passed
Block-frequency	0.858668	0.901254	0.854725	Passed
Universal	0.723179	0.245789	0.632548	Passed
Rank	0.725031	0.325684	0.125487	Passed
Longest runs of ones	0.901256	0.412578	0.754213	Passed
Runs	0.512489	0.854124	0.754968	Passed
Random excursions x=1	0.965412	0.845217	0.124854	Passed
Linear complexity	0.845236	0.125786	0.452136	Passed
Cumulative sums (reverse)	0.124785	0.856127	0.185429	Passed
Cumulative sums (forward)	0.945281	0.425815	0.754621	Passed
Random excursions variant x=1	0.753146	0.245701	0.356721	Passed
Approximate entropy	0.845621	0.125875	0.654280	Passed

(a) -Data1	(b) -Data2	(c) -Data3	(d) -Data4

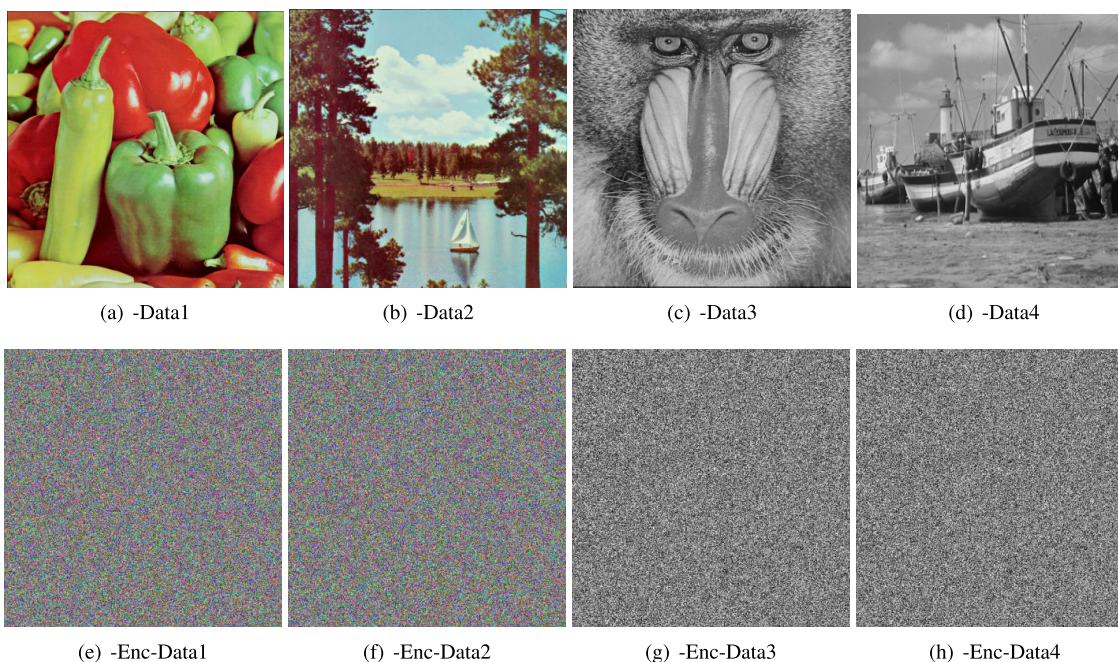| (e) -Enc-Data1	(f) -Enc-Data2	(g) -Enc-Data3	(h) -Enc-Data4

FIGURE 13. Visual test of the dataset images. It is observed that the plain images are no more recognizable after encryption.

correlation coefficients of the original images are close to 1, whereas those of the encrypted images close to 0. This shows that the encryption algorithm has considerably attenuated the correlation between the pixels of the encrypted images. Figure 14 presents the correlation distributions of adjacent pixels in horizontal, vertical and diagonal directions for both original color data and corresponding cipher data. Figure 15 presents the correlation distributions of adjacent pixels in horizontal (H), vertical (V) and diagonal (D) directions for

both original color data and corresponding cipher data. These outcomes also confirm that the encrypted images are heavily decorrelated.

2) GLOBAL AND LOCAL ENTROPY TESTS
Global and local entropy are two important indicators used for random characteristics of a cryptosystem. The greater the information entropy, the more uncertain the information we
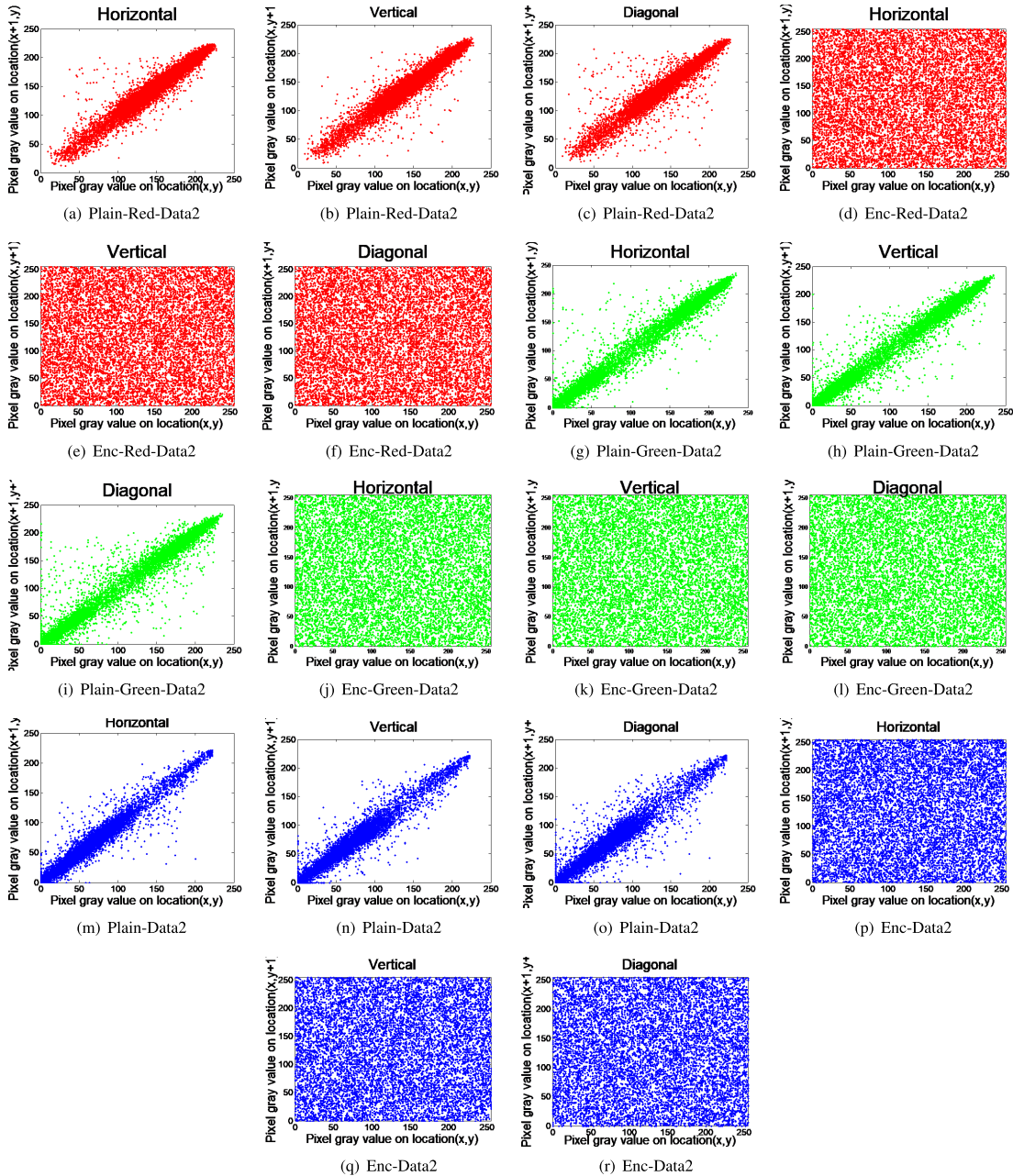
FIGURE 14. Distribution of correlation for color plain data2 and corresponding cipher.

TABLE 3. Correlation coefficients in horizontal (H), vertical (V) and diagonal (D) directions for both original color data and corresponding cipher data.

Colour data	directions	R		G		B	
		Original	Encrypted	Original	Encrypted	Original	Encrypted
Data 1	H	0.9564	0.0206	0.9689	-0.0112	0.9713	0.0110
	V	0.9568	0.0003	0.9721	0.0107	0.9739	-0.0069
	D	0.9464	-0.0141	0.9553	-0.0039	0.9574	0.0269
Data 2	H	0.9675	-0.0045	0.9843	0.0142	0.9694	0.0005
	V	0.9666	0.0001	0.9813	-0.0085	0.9698	-0.0018
	D	0.9590	0.0079	0.9710	0.0079	0.9542	-0.0264

TABLE 4. Correlation coefficients of original and encrypted Grey-scale data.

Grey-scale data	Plan	Original	Encrypted
Data 3	H	0.7577	-0.0036
	V	0.8690	0.0015
	D	0.7290	-0.0151
Data 4	H	0.9931	0.0068
	V	0.9856	-0.0049
	D	0.9787	-0.0023

have [76]. It can be evaluated as follows:

$$E(x_i) = -\sum_{i=0}^{255} p(x_i)\, log_2\, p(x_i), \quad (20)$$

where $p(x_i)$ represents the probability of the gray level $x_{(i)}$. Global and local entropy are evaluated for our test images and recovered in TABLE 5. The images having 2^8 possible
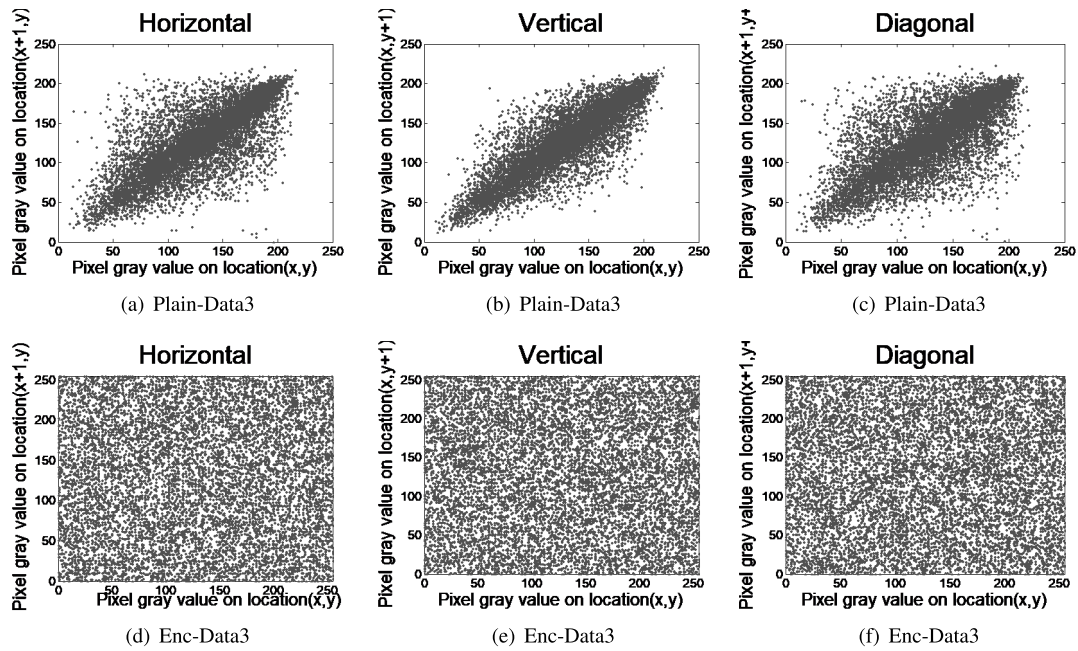
FIGURE 15. Distribution of correlation for gay-scale plain data3 and corresponding cipher.

TABLE 5. Global and local entropy of each encrypted test data.

Data	Global entropy	Local entropy
Enc-Data1	7.9998	7.9039
Enc-Data2	7.9997	7.9022
Enc-Data3	7.9992	7.9024

values, the ideal entropy value is equal to 8 bits. With regard to the entropy values in TABLE 5 it is observed that entropy values for the cipher data are very close to TABLE 10. Thus, the proposed algorithm is secure against entropy based attacks.

3) HISTOGRAM, χ^2 AND VARIANCE TESTS

Any good encryption scheme must pass the histogram and chi-square test to be able to resist the statistical intrusion of a third party [77]. The histogram of a plain data is usually distributed randomly whereas the histogram of the corresponding cipher is required to be uniform. Figures 16 and 17 present the histograms of the plain and cipher color and gray scale images. It is obvious to observe that the histograms of the plain image are randomly distributed while the histograms of the encrypted data are flat. This flatness can be checked using the chi-square test. TABLE 6 provides the issue of chi-square values with 0.05 as weight value. Usually, the flatness of the histogram is validated if the chi-square value of the test sample is less than 293.2478 indicating a p-value higher than 0.5. Regarding TABLE 6 the histograms of various test samples are validated. Variance of histogram is another metric currently used to evaluate the uniformity

of encrypted image [78]. this metric can be computed with respect to encryption keys using the following formula:

$$v(H) = \frac{1}{m \times n} \sum_{i=1}^{m} \sum_{j=1}^{n} \frac{1}{2}(h_i - h_j)^2 \qquad (21)$$

where $H = \{h_1, h_2, \ldots\ldots, h_{256}\}$ is a vector containing the values of pixels. Considering a key set comprising 8 keys as $\tilde{\phi}, \tilde{y}, \tilde{u}, A, B, C, f_0, \omega$ a cipher image is obtained and the variance is computed using Eq. 21. One of the elements of the key set is changed to form a new key set in order to produce a new cipher and compute its. The results are summarized in Table 7 where each column indicate the results of variances when only one element of the key set is changed to form a new key set. From the results of Table 7 the variances of the cipher images are very close indicating the uniformity of the encrypted data obtained from diffferent keys.

4) NPCR AND UACI TESTS

To assess the capability of an encryption algorithm to withstand differential attacks NPCR (Number of Pixels Change Rate) and UACI are commonly used [79]. These metrics evaluate the rate of change in the original image on its equivalent cipher one. The numerical value of NPCR is computed as:

$$NPCR = \frac{\sum_{m,n} Diff(m, n)}{D} \times 100\%,$$

$$Diff(m, n) = \begin{cases} 0, & if \ P(m, n) = C(m, n) \\ 1, & if \ P(m, n) \neq C(m, n) \end{cases} \qquad (22)$$

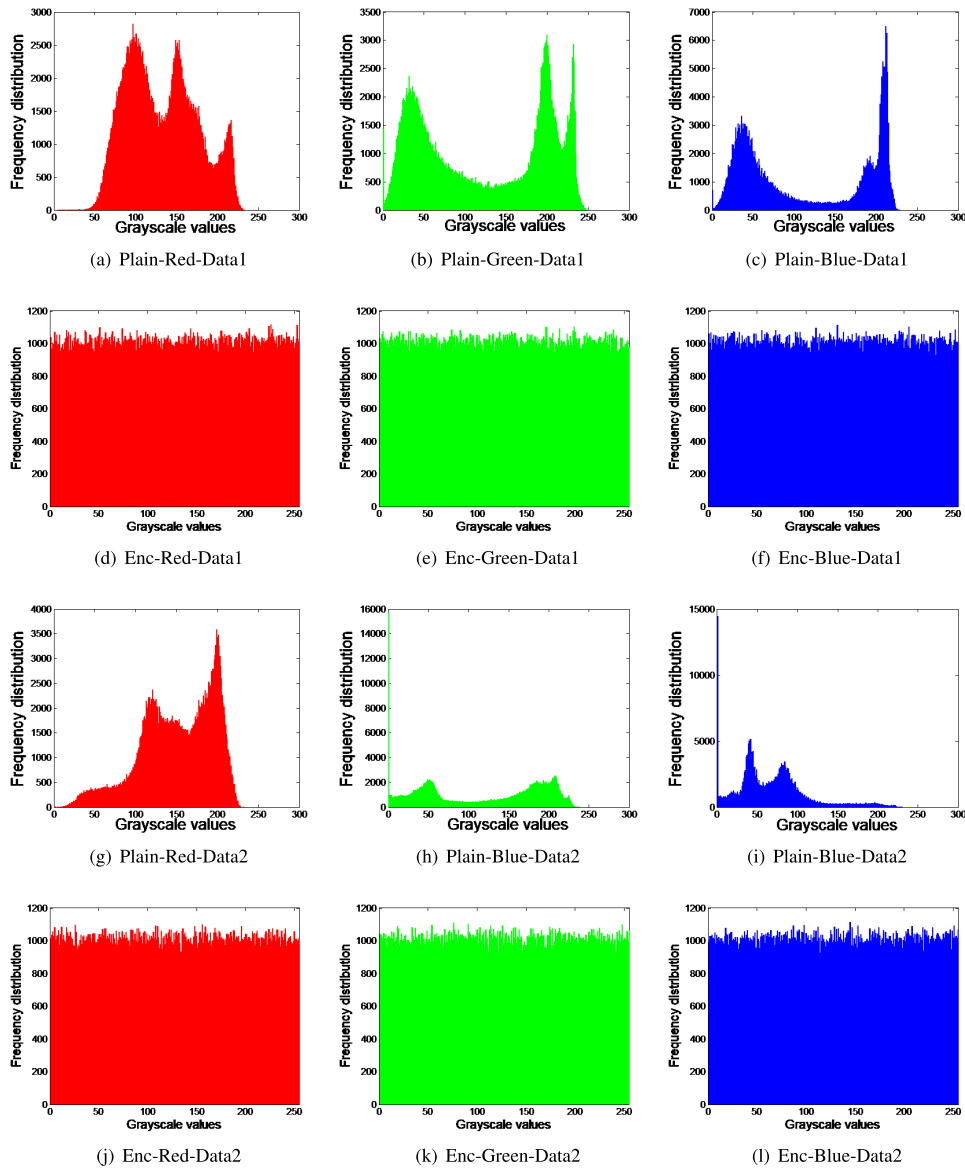here D indicates to the complete pixel numbers in the image. On the other hand numerical value of *UACI* is

(a) Plain-Red-Data1 (b) Plain-Green-Data1 (c) Plain-Blue-Data1

(d) Enc-Red-Data1 (e) Enc-Green-Data1 (f) Enc-Blue-Data1

(g) Plain-Red-Data2 (h) Plain-Blue-Data2 (i) Plain-Blue-Data2

(j) Enc-Red-Data2 (k) Enc-Green-Data2 (l) Enc-Blue-Data2

FIGURE 16. Histograms for each color plain data set and its corresponding cipher.
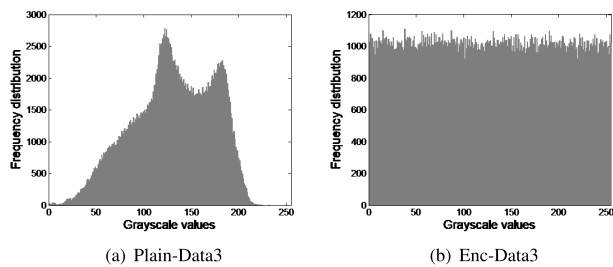

(a) Plain-Data3 (b) Enc-Data3

FIGURE 17. Histograms for each grey-scale plain data set and its corresponding cipher.

computed as:

$$UACI = \frac{100}{m \times n} \sum_{1}^{m} \sum_{1}^{n} \frac{|IC_1(m, n) - IC_2(m, n)|}{255}, \quad (23)$$

TABLE 6. χ^2 values for each encrypted data.

Data	χ^2 values				Decision
	R	G	B	Average	
Data1	196697.3066	130154.7167	344571.5371	223807.8535	Non-uniform
Enc-Data1	249.8242	233.0878	226.1660	236.3593	Uniform
Data2	213187.2167	318382.9296	49142.81777	340999.4414	Non-uniform
Enc-Data2	251.1250	274.2363	248.2167	257.8593	Uniform
Data3	-	-	-	187692.1718	Non-uniform
Enc-Data3	-	-	-	276.0292	Uniform

where IC_1 and IC_2 are two encrypted images obtained from ciphers images different in just on pixel. m and n are the dimension of the images.

The outcomes of NPCR and UACI for the experimented dataset are displayed in TABLE 8. From these results, the given encryption approach has a high sensitivity to tiny

TABLE 7. Outcome of variance analysis for different key sets.

Encrypted image	K_A	K_B	K_C	K_f0
Enc-Data1	250.95	248.54	252.19	250.35
Enc-Data2	249.24	250.46	250.52	253.42
Enc-Data3	252.12	251.54	254.34	255.95
Enc-Data4	251.35	249.42	250.91	242.23

TABLE 8. NPCR and UACI values for encrypted dataset.

Data3	NPCR %	UACI %
Enc-Data1	99.61509	33.48937
Enc-Data2	99.61090	33.51067
Enc-Data3	99.61281	33.43230

pixel changes in the original image. Consequently, encrypted images are secured against any form of differential attacks.

5) KEY SPACE ANALYSIS

The key space of an encryption algorithm is the product of all the keys used in the encryption process ($Ks = \Pi_{i=1}^{n} k_i$ where Ks is the key space and k_i are the keys related to the encryption process) [80]. The key space of a good encryption should be greater than 2^{100} so that the algorithm can resist to brute force attacks. For this case we considered 8 keys ($\tilde{\phi}$, $\tilde{y}$, $\tilde{u}$, A, B, C, f_0, ω). If the calculation accuracy of each key is considered to be 10^{16} then the key space of the whole algorithm is 10^{128}. This value is greater than the threshold value (2^{100}) consequently the considered algorithm can resist to brute force attacks based on the analysis of keys. Let us mention that when initial conditions are used as key for any encryption algorithm, special care need to be taken to avoid non-chaotic [81].

6) KEY SENSITIVITY ANALYSIS

Any cryptosystem is required to be sensitive to tiny change in the keys that is any slight change in the key should cause significant effect in the encrypted data [2]. To test the sensitivity of our algorithm to keys a given plain image is encrypted using correct key. Then correct key ($A = 0.4490$; $B = -1.5998$; $C = -3.7125$; $f_0 = 1.9$; $\tilde{\phi} = -0.0524$; $\tilde{y} = -0.2$; $\tilde{u} = 0$)is successfully to decrypt the cipher data but a slighly set of modified keys are used unsuccessfully to decrypt the cipher data. Figure 18 summarized the results of key sensitivity tests.

7) NOISE ATTACK ANALYSIS

Salt-and-pepper and Gaussian are two types of noises currently encountered in image processing. This part aims to verify if the proposed encryption algorithm is able to resist to such type of noises [9]. In this line a certain amount of Gaussian noise and salt-and-pepper noises are added to the encrypted data. The proposed encryption algorithm is then used to decrypt the infected images. Figures 19 and 20 show that our algorithm is able to produce readable image from

(a) - Correct key   (b) - Correct key with A=0.449000000000001

(c) - Correct key with f_0= 1.90000000001   (d)- Correct key with y_0 = - 0.20000000001

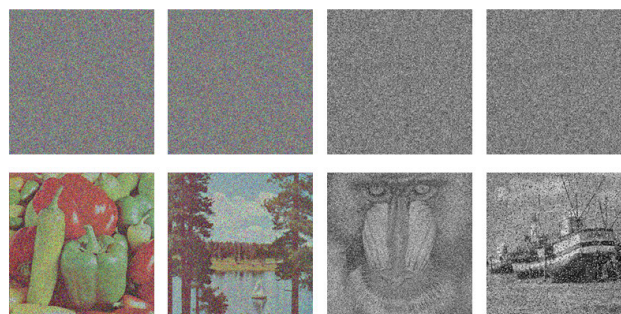**FIGURE 18.** Outcomes of key sensitivity analysis.

FIGURE 19. Salt-and-pepper noise analysis: the first line presents the noise infected images with 0.5 as parameter and the second line indicate the corresponding decrypted images.

FIGURE 20. Gaussian noise analysis: the first line presents the noise infected images with 0.5 as parameter and the second line indicate the corresponding decrypted images.
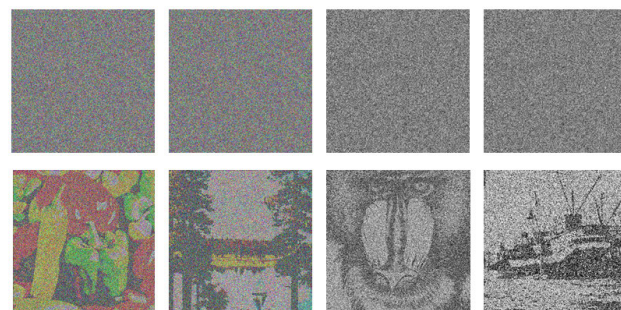
infected cipher. the proposed encryption algorithm is more efficient on Salt-and-pepper noise.

8) OCCLUSION ATTACK ANALYSIS

Images usualy loss some informations during the transmission process. This is called occlusion attack and a
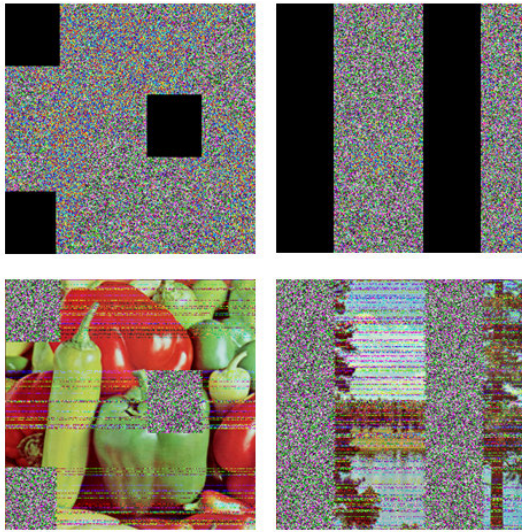
FIGURE 21. Outcomes of occlusion attacks.

TABLE 9. Computational time (in milliseconds) for various size test images and comparison with existing works.

Algorithm	Data1			Data1			Data1		
	256 × 256	512 × 512	1024 × 1024	256 × 256	512 × 512	1024 × 1024	256 × 256	512 × 512	1024 × 1024
Proposed	**1.23**	**3.17**	**12.72**	**1.70**	**3.81**	**13.91**	**2.21**	**6.48**	**14.59**
[85]	7.79	31.10	124.64	5.82	28.09	120.42	9.80	38.07	129.43
[59]	4.60	18.06	54.35	3.86	12.49	50.15	8.21	27.92	61.02
[86]	1270	5070	20560	986.05	40256	17285	1586	8459	25785

MATLAB while ET and NC are computed as:

$$ET = \frac{size\ of\ the\ image(Byte)}{Encryption\ time\ (sec)} \qquad (24)$$

$$NC = \frac{CPU\ speed\ (Hz)}{ET\ (Byte/sec)} \qquad (25)$$

A good encryption algorithm is required to take less encryption time, less NC, and high ET to be suitable for real time implementation. TABLE 9 contains the running time of the encryption algorithm while using the various size of test image "*Data1*" (example 512 × 512 × 3 bytes). On the other hand TABLE 9 provides the ET and the NC computed with 512 × 512 × 3 bytes version of "*Data1*". The computational workstation is characterized by 2.4GHz processor Intel core TM i7-3630QM 16 GB RAM and MATLAB R2014b software. The computational time increases with respect to the size of the plain image. Note this computational time also relies on the capacity of the workstation (the processor speed and the RAM). It is clearly seen from TABLE 9 and TABLE 10 that an acceptable complexity is obtained and the algorithm is competitive with some fastest chaos-based cryptosystems results of the state of the art.

TABLE 10. ET and NC computed with 512 × 512 × 3 bytes version of Img01.

Algorithm	ET (MBps)	NC
Proposed	**248.08**	**9,67**
[85]	24.06	122.85
[59]	41.52	62.00
[86]	0.14	94.60

well-designed encryption/decryption algorithm should be able to withstand such type of attack. To test the capability of the proposed algorithm to resist occlusion a dark matrix is created on the encrypted image. Then the proposed method is used to decrypt the attacked image. From the results of Figure 21 the recovered image is readable. Consequently the occlusion does not affect the decryption.

9) CLASSICAL TYPES OF ATTACK
Any encryption algorithm should be able to resist to the four classical forms of attacks such as ciphertext only (The hacker has a part of the encrypted data), known plaintext (The hacker has a part of the plain data and the corresponding encrypted data), chosen ciphertext (The hacker has the possibilty to choose a part of the plain data and construct the corresponding cipher data using the algorithm), chosen plaintext (The hacker has the possibilty to choose a part of the cipher data and construct the corresponding plain data using the algorithm) [10]. It is obvious that a given cryptosystem is robust to any form of the above described attacks if it resists to chosen plaintext attack. The algorithm proposed in this paper is sensitive to any change in chaotic system parameters and initial seeds. In addition the encrypted data also depends on the plain data as we use Hash algorithm with plain data as input to compute the initial seed of the chaotic system. Consequently even with a part of the plain data and cipher data our algorithm can resist to chosen plaintext attack.

10) COMPLEXITY ANALYSIS
Complexity analysis is one of the most important tools to measure the performance of an algorithm. [82]–[85] This complexity can be computed in terms of running time or the Encryption Throughput (ET) and the Number of Cycles (NC) required securing one byte of the plain image. Note that the encryption time is computed using the "*tic-toc*" function of

11) COMPARISON ANALYSIS
A variety of chaos based encryption techniques can be found in the literature. In this part a comparative analysis between the proposed techniques and some recent literature is done. TABLE 11 show the outcome of comparative analysis in terms of some well-known metrics including NPCR, UACI, information entropy, algorithm complexity. Our algorithm shows the highest NPCR and entropy compared to some recents achievements in the literature. In the case of UACI our result is poor compare to the results in some recents achievements of the literature but the value of UACI achieved by our work is above the threshold value which is 33.46354% regarding the correlation the values achieved by our algorithm are more closed to 0 than the values in some recent works in the literature. Table 10 shows the outcome of comparative analysis in terms of algorithm complexity. As mentioned

TABLE 11. Outcome of comparative analysis.

	NPCR (%)	UACI (%)	Entropy	Time (seconds)	Correlation Coefficients		
					H	V	D
This work	99.61509	33.51067	7.9998	0.0317	0.0206	0.0003	-0.0141
[87]	99.6030	33.552	-	0.5156	0.0190	0.0009	0.0003
[88]	99.5990	33.290	-	25.3077	0.0160	0.0012	0.0011
[89]	89.4150	33.698	-	0.6132	0.0125	0.0011	0.0004
[90]	99.6090	33.387	-	8.6154	0.0120	0.0013	0.0015
[91]	99.6180	33.521	7.9993	0.6212	0.0208	0.0009	0.0021
[92]	99.6800	33.7900	7.9973	-	0.0082	0.0079	0.0066

above a good encryption algorithm is required to take less encryption time, less NC, and high ET to be suitable for real time implementation. It is clear from this result that our algorithm achieve the smallest encryption time and NC but the highest ET compared to some recents achievements in the literature.

VI. CONCLUSION

The supernonlinear and nonlinear periodic IAWs have been investigated in a nonextensive plasma system which is composed of pair ions (positive and negative) through the direct approach. Dynamical system has been formed directly from the model equations applying the suitable transformation. To examine dynamical behaviors, the existing DS has been disturbed with external periodic force. The DS and perturbed DS have been studied considering suitable values of physical parameters. The solitary, supernonlinear and nonlinear periodic IAW solutions have been shown through phase plane analysis for the DS. The periodic wave solution for IAW has been obtained analytically. It has been observed numerically that the SPIAW and NPIAW have become spiky and smooth according to $q \rightarrow \infty$ and $V \rightarrow \infty$. Furthermore, the dynamical features such as chaos, various forms of quasiperiodic and multiperiodic orbits have been discovered under the perturbed DS. Multistability property of IAWs has been featured with coexisting trajectories such as, quasiperiodic, multiperiodic and chaotic trajectories with same parametric values but at different initial conditions. The coexistence of such dynamical features has been verified by their corresponding phase and time series plots. The positive values of Lyapunov exponents have been presented for the chaotic feature. Suitable parameter values of space plasma [22], [56] have been used in the present work. Chaotic dynamics of the proposed IAWs system have been exploited to design efficient encryption algorithm. The security performance has been evaluated using some well-known metrics and obtained results have indicated that the proposed cryptosystem can resist most of existing cryptanalysis techniques. In addition complexity analysis shows the possibility of practical implementation of the proposed algorithm.

REFERENCES

[1] X.-Y. Wang, L. Yang, R. Liu, and A. Kadir, "A chaotic image encryption algorithm based on perceptron model," *Nonlinear Dyn.*, vol. 62, no. 3, pp. 615–621, Nov. 2010.

[2] Y.-Q. Zhang and X.-Y. Wang, "A new image encryption algorithm based on non-adjacent coupled map lattices," *Appl. Soft Comput.*, vol. 26, pp. 10–20, Jan. 2015.

[3] H. Liu and X. Wang, "Color image encryption based on one-time keys and robust chaotic maps," *Comput. Math. Appl.*, vol. 59, no. 10, pp. 3320–3327, May 2010.

[4] H. Liu, X. Wang, and A. Kadir, "Image encryption using DNA complementary rule and chaotic maps," *Appl. Soft Comput.*, vol. 12, no. 5, pp. 1457–1466, May 2012.

[5] Z.-L. Zhu, W. Zhang, K.-W. Wong, and H. Yu, "A chaos-based symmetric image encryption scheme using a bit-level permutation," *Inf. Sci.*, vol. 181, no. 6, pp. 1171–1186, Mar. 2011.

[6] H. Liu and X. Wang, "Color image encryption using spatial bit-level permutation and high-dimension chaotic system," *Opt. Commun.*, vol. 284, nos. 16–17, pp. 3895–3903, Aug. 2011.

[7] Y. Xian and X. Wang, "Fractal sorting matrix and its application on chaotic image encryption," *Inf. Sci.*, vol. 547, pp. 1154–1169, Feb. 2021.

[8] X. Wang and S. Gao, "Image encryption algorithm based on the matrix semi-tensor product with a compound secret key produced by a Boolean network," *Inf. Sci.*, vol. 539, pp. 195–214, Oct. 2020.

[9] X. Wang, L. Feng, and H. Zhao, "Fast image encryption algorithm based on parallel computing system," *Inf. Sci.*, vol. 486, pp. 340–358, Jun. 2019.

[10] X. Wang, L. Teng, and X. Qin, "A novel colour image encryption algorithm based on chaos," *Signal Process.*, vol. 92, no. 4, pp. 1101–1108, Apr. 2012.

[11] Q. Lai, T. Nestor, J. Kengne, and X.-W. Zhao, "Coexisting attractors and circuit implementation of a new 4D chaotic system with two equilibria," *Chaos, Solitons Fractals*, vol. 107, pp. 92–102, Feb. 2018.

[12] J. Kengne, N. Tsafack, and L. K. Kengne, "Dynamical analysis of a novel single opamp-based autonomous LC oscillator: Antimonotonicity, chaos, and multiple attractors," *Int. J. Dyn. Control*, vol. 6, no. 4, pp. 1543–1557, Mar. 2018.

[13] J. Jacquinot, B. D. McVey, and J. E. Scharer, "Mode conversion of the fast magnetosonic wave in a deuterium-hydrogen tokamak plasma," *Phys. Rev. Lett.*, vol. 39, no. 2, pp. 88–91, Jul. 1977.

[14] R. A. Gottscho and C. E. Gaebe, "Negative ion kinetics in RF glow discharges," *IEEE Trans. Plasma Sci.*, vol. 14, no. 2, pp. 92–102, Apr. 1986.

[15] H. Saleem, "A criterion for pure pair-ion plasmas and the role of quasineutrality in nonlinear dynamics," *Phys. Plasmas*, vol. 14, no. 1, Jan. 2007, Art. no. 014505.

[16] S. K. El-Labany, S. A. El-Warraki, and W. M. Moslem, "Cylindrical ion-acoustic waves in a warm multicomponent plasma," *J. Plasma Phys.*, vol. 63, no. 4, pp. 343–352, May 2000.

[17] M. Tribeche and M. Benzekka, "Nonlinear dust acoustic waves in electronegative dusty plasmas," *Astrophys. Space Sci.*, vol. 331, no. 2, pp. 619–626, Feb. 2011.

[18] E. K. El-Shewy, "Effect of the presence of excess superthermal hot electrons on electron-acoustic solitary waves in auroral zone plasma," *Astrophys. Space Sci.*, vol. 335, no. 2, pp. 389–397, Oct. 2011.

[19] E. K. El-Shewy, M. I. A. El Maaty, H. G. Abdelwahed, and M. A. Elmessary, "Solitary solution and energy for the Kadomstev–Petviashvili equation in two temperatures charged dusty grains," *Astrophys. Space Sci.*, vol. 332, no. 1, pp. 179–186, Mar. 2011.

[20] S. A. El-Tantawy and W. M. Moslem, "Nonlinear electrostatic excitations in electron-depleted electronegative dusty plasma with two-negative ion species," *Astrophys. Space Sci.*, vol. 337, no. 1, pp. 209–215, Sep. 2011.

[21] P. H. Chaizy, H. Rème, J. A. Sauvaud, C. d'Uston, R. P. Lin, D. E. Larson, D. L. Mitchell, K. A. Anderson, C. W. Carlson, A. Korth, and D. A. Mendis, "Negative ions in the coma of comet Halley," *Nature*, vol. 349, no. 6308, pp. 393–396, Jan. 1991.

[22] A. J. Coates, F. J. Crary, G. R. Lewis, D. T. Young, J. H. Waite, and E. C. Sittler, "Discovery of heavy negative ions in Titan's ionosphere," *Geophys. Res. Lett.*, vol. 34, no. 22, Nov. 2007.

[23] A. Lavagno, G. Kaniadakis, M. Rego-Monteiro, P. Quarati, and C. Tsallis, "Non-extensive thermostatistical approach of the peculiar velocity function of galaxy clusters," *Astrophys. Lett. Commun.*, vol. 35, p. 449, Jul. 1998.

[24] B. M. Boghosian, "Thermodynamic description of the relaxation of two-dimensional turbulence using Tsallis statistics," *Phys. Rev. E, Stat. Phys. Plasmas Fluids Relat. Interdiscip. Top.*, vol. 53, p. 4754, May 1996.

[25] C. Tsallis, "Possible generalization of Boltzmann-gibbs statistics," *J. Stat. Phys.*, vol. 52, nos. 1–2, pp. 479–487, Jul. 1988.

[26] C. Tsallis and D. J. Bukman, "Anomalous diffusion in the presence of external forces: Exact time-dependent solutions and their thermostatistical basis," *Phys. Rev. E, Stat. Phys. Plasmas Fluids Relat. Interdiscip. Top.*, vol. 54, no. 3, pp. R2197–R2200, Sep. 1996.

[27] M. P. Leubner, "A nonextensive entropy approach to kappa-distributions," *Astrophys. Space Sci.*, vol. 282, pp. 573–579, Feb. 2002.

[28] B. Liu and J. Goree, "Superdiffusion and non-Gaussian statistics in a driven-dissipative 2D dusty plasma," *Phys. Rev. Lett.*, vol. 100, no. 5, Feb. 2008, Art. no. 055003.

[29] M. P. Almeida, "Generalized entropies from first principles," *Phys. A, Stat. Mech. Appl.*, vol. 300, nos. 3–4, pp. 424–432, Nov. 2001.

[30] J. Du, "Nonextensivity in nonequilibrium plasma systems with Coulombian long-range interactions," *Phys. Lett. A*, vol. 329, nos. 4–5, pp. 262–267, Aug. 2004.

[31] D. Jiulin, "Nonextensivity and the power-law distributions for the systems with self-gravitating long-range interactions," *Astrophys. Space Sci.*, vol. 312, nos. 1–2, pp. 47–55, Nov. 2007.

[32] A. E. Dubinov and D. Y. Kolotkov, "Ion-acoustic super solitary waves in dusty multispecies plasmas," *IEEE Trans. Plasma Sci.*, vol. 40, no. 5, pp. 1429–1433, Apr. 2012.

[33] A. E. Dubinov and D. Y. Kolotkov, "Interpretation of ion-acoustic solitons of unusual form in experiments in SF6-ar plasma," *High Energy Chem.*, vol. 46, no. 6, pp. 349–353, Nov. 2012.

[34] A. E. Dubinov and D. Y. Kolotkov, "Ion-acoustic supersolitons in plasma," *Plasma Phys. Rep.*, vol. 38, no. 11, pp. 909–912, Nov. 2012.

[35] F. Verheest, "Nonlinear acoustic waves in nonthermal plasmas with negative and positive dust," *Phys. Plasmas*, vol. 16, no. 1, Jan. 2009, Art. no. 013704.

[36] T. K. Baluku, M. A. Hellberg, and F. Verheest, "New light on ion acoustic solitary waves in a plasma with two-temperature electrons," *EPL (Europhys. Lett.)*, vol. 91, no. 1, p. 15001, Jul. 2010.

[37] O. R. Rufai, R. Bharuthram, S. V. Singh, and G. S. Lakhina, "Ion acoustic solitons and supersolitons in a magnetized plasma with nonthermal hot electrons and Boltzmann cool electrons," *Phys. Plasmas*, vol. 21, no. 8, Aug. 2014, Art. no. 082304.

[38] G. S. Lakhina, S. V. Singh, and A. P. Kakad, "Ion acoustic solitons/double layers in two-ion plasma revisited," *Phys. Plasmas*, vol. 21, no. 6, Jun. 2014, Art. no. 062311.

[39] S. A. El-Wakil, E. M. Abulwafa, and A. A. Elhanbaly, "Super-soliton dust-acoustic waves in four-component dusty plasma using non-extensive electrons and ions distributions," *Phys. Plasmas*, vol. 24, no. 7, Jul. 2017, Art. no. 073705.

[40] S. H. Strogatz, *Nonlinear Dynamics and Chaos*. Boulder, CO, USA: Westview Press, 2007.

[41] J. K. Hale and S.-N. Chow, *Methods of Bifurcation Theory*. New York, NY, USA: Springer-Verlag, 1982.

[42] J. Guckenheimer and P. Holmes, *Nonlinear Oscillations, Dynamical Systems, and Bifurcations of Vector Fields*. New York, NY, USA: Springer-Verlag, 1983.

[43] U. Kumar Samanta, A. Saha, and P. Chatterjee, "Bifurcations of dust ion acoustic travelling waves in a magnetized dusty plasma with aq-nonextensive electron velocity distribution," *Phys. Plasmas*, vol. 20, no. 2, Feb. 2013, Art. no. 022111.

[44] S. K. El-Labany, W. F. El-Taibany, and A. Atteya, "Bifurcation analysis for ion acoustic waves in a strongly coupled plasma including trapped electrons," *Phys. Lett. A*, vol. 382, no. 6, pp. 412–419, Feb. 2018.

[45] S. Y. El-Monier and A. Atteya, "Bifurcation analysis for dust-acoustic waves in a four-component plasma including warm ions," *IEEE Trans. Plasma Sci.*, vol. 46, no. 4, pp. 815–824, Apr. 2018.

[46] R. A. Shahein and A. R. Seadawy, "Bifurcation analysis of KP and modified KP equations in an unmagnetized dust plasma with nonthermal distributed multi-temperatures ions," *Indian J. Phys.*, vol. 93, no. 7, pp. 941–949, Jul. 2019.

[47] A. Saha and P. Chatterjee, "Solitonic, periodic, quasiperiodic and chaotic structures of dust ion acoustic waves in nonextensive dusty plasmas," *Eur. Phys. J. D*, vol. 69, no. 9, p. 203, Sep. 2015.

[48] M. F. Abdul Rahim, H. Natiq, N. A. A. Fataf, and S. Banerjee, "Dynamics of a new hyperchaotic system and multistability," *Eur. Phys. J. Plus*, vol. 134, no. 10, p. 499, Oct. 2019.

[49] S. He, S. Banerjee, and K. Sun, "Complex dynamics and multiple coexisting attractors in a fractional-order microscopic chemical system," *Eur. Phys. J. Special Topics*, vol. 228, no. 1, pp. 195–207, May 2019.

[50] H. Natiq, S. Banerjee, A. P. Misra, and M. R. M. Said, "Degenerating the butterfly attractor in a plasma perturbation model using nonlinear controllers," *Chaos, Solitons Fractals*, vol. 122, pp. 58–68, May 2019.

[51] H. Natiq, S. Banerjee, M. R. K. Ariffin, and M. R. M. Said, "Can hyperchaotic maps with high complexity produce multistability?" *Chaos, Interdiscipl. J. Nonlinear Sci.*, vol. 29, no. 1, Jan. 2019, Art. no. 011103.

[52] H. Natiq, M. R. M. Said, M. R. K. Ariffin, S. He, L. Rondoni, and S. Banerjee, "Self-excited and hidden attractors in a novel chaotic system with complicated multistability," *Eur. Phys. J. Plus*, vol. 133, no. 12, p. 557, Dec. 2018.

[53] A. Saha, B. Pradhan, and S. Banerjee, "Multistability and dynamical properties of ion-acoustic wave for the nonlinear Schrödinger equation in an electron–ion quantum plasma," *Phys. Scripta*, vol. 95, no. 5, p. 055602, Feb. 2020.

[54] B. Yan, P. K. Prasad, S. Mukherjee, A. Saha, and S. Banerjee, "Dynamical complexity and multistability in a novel lunar wake plasma system," *Complexity*, vol. 2020, pp. 1–11, Mar. 2020, doi: 10.1155/2020/5428548.

[55] A. Abdikian, J. Tamang, and A. Saha, "Electron-acoustic supernonlinear waves and their multistability in the framework of the nonlinear Schrödinger equation," *Commun. Theor. Phys.*, vol. 72, no. 7, Jun. 2020, Art. no. 075502.

[56] S. K. El-Labany, W. M. Moslem, N. A. El-Bedwehy, R. Sabry, and H. N. A. El-Razek, "Rogue wave in Titan's atmosphere," *Astrophys. Space Sci.*, vol. 338, no. 1, pp. 3–8, Mar. 2012.

[57] T. Habutsu, Y. Nishio, I. Sasase, and S. Mori, "A secret key cryptosystem by iterating a chaotic map," in *Proc. Workshop Theory Appl. Cryptograph. Techn.* Cham, Switzerland: Springer, 1991, pp. 127–140.

[58] E. Biham and A. Shamir, "Differential cryptanalysis of DES-like cryptosystems," *J. Cryptol.*, vol. 4, no. 1, pp. 3–72, Jan. 1991.

[59] M. S. Baptista, "Cryptography with chaos," *Phys. Lett. A*, vol. 240, pp. 50–54, Mar. 1998.

[60] K. C. Jithin and S. Sankar, "Colour image encryption algorithm combining arnold map, DNA sequence operation, and a mandelbrot set," *J. Inf. Secur. Appl.*, vol. 50, Feb. 2020, Art. no. 102428.

[61] A. S. Bains, M. Tribeche, and T. S. Gill, "Modulational instability of ion-acoustic waves in a plasma with a q-nonextensive electron velocity distribution," *Phys. Plasmas*, vol. 18, no. 2, Feb. 2011, Art. no. 022108.

[62] L. Ait Gougam and M. Tribeche, "Ion-acoustic soliton energy in a plasma with nonextensive electrons," *Phys. A, Stat. Mech. Appl.*, vol. 407, pp. 226–230, Aug. 2014.

[63] S. A. El-Tantawy, E. I. El-Awady, and M. Tribeche, "On the rogue waves propagation in non-maxwellian complex space plasmas," *Phys. Plasmas*, vol. 22, no. 11, Nov. 2015, Art. no. 113705.

[64] S. A. El-Tantawy, "Effect of ion viscosity on dust ion-acoustic shock waves in a nonextensive magnetoplasma," *Astrophys. Space Sci.*, vol. 361, no. 8, p. 249, Jul. 2016.

[65] Z. Fu, S. Liu, S. Liu, and Q. Zhao, "New jacobi elliptic function expansion and new periodic solutions of nonlinear wave equations," *Phys. Lett. A*, vol. 290, nos. 1–2, pp. 72–76, Nov. 2001.

[66] A. Saha and P. Chatterjee, "Bifurcations of ion acoustic solitary waves and periodic waves in an unmagnetized plasma with kappa distributed multi-temperature electrons," *Astrophys. Space Sci.*, vol. 350, no. 2, pp. 631–636, Jan. 2014.

[67] A. Saha and P. Chatterjee, "Qualitative structures of electron-acoustic waves in an unmagnetized plasma with q-nonextensive hot electrons," *Eur. Phys. J. Plus*, vol. 130, no. 11, p. 222, Nov. 2015.

[68] A. Saha and J. Tamang, "Effect of q-nonextensive hot electrons on bifurcations of nonlinear and supernonlinear ion-acoustic periodic waves," *Adv. Space Res.*, vol. 63, no. 5, pp. 1596–1606, Mar. 2019.

[69] A. Sen, S. Tiwari, S. Mishra, and P. Kaw, "Nonlinear wave excitations by orbiting charged space debris objects," *Adv. Space Res.*, vol. 56, no. 3, pp. 429–435, Aug. 2015.

[70] L. Mandi, A. Saha, and P. Chatterjee, "Dynamics of ion-acoustic waves in Thomas-Fermi plasmas with source term," *Adv. Space Res.*, vol. 64, no. 2, pp. 427–435, Jul. 2019.

[71] N. Tsafack and J. Kengne, *A Particular Class of Simple Chaotic Circuits: Multistability Analysis*. Riga, Latvia: Lap LAMBERT Academic Publishing, 2019.

[72] N. Tsafack and J. Kengne, "Multiple coexisting attractors in a generalized Chua's circuit with a smoothly adjustable symmetry and nonlinearity," *J. Phys. Math.*, vol. 10, no. 298, pp. 0902–2090, 2019.

[73] N. Tsafack and J. Kengne, "Complex dynamics of the Chua's circuit system with adjustable symmetry and nonlinearity: Multistability and simple circuit realization," *World J. Appl. Phys.*, vol. 4, no. 2, pp. 24–34, Sep. 2019, doi: 10.11648/j.wjap.20190402.12.

[74] S. Long, "A comparative analysis of the application of hashing encryption algorithms for MD5, SHA-1, and SHA-512," *J. Phys., Conf. Ser.*, vol. 13149, Oct. 2019, Art. no. 012210, doi: 10.1088/1742-6596/1314/1/012210.

[75] J. Nkapkop, J. Effa, M. Borda, and R. Terebes, "A novel fast and secure chaos-based algorithm for image encryption," in *Proc. Int. Conf. Inf. Technol. Commun.* Cham, Switzerland: Springer, vol. 9522, Jan. 2015, pp. 87–101.

[76] X. Wang, C. Liu, and H. Zhang, "An effective and fast image encryption algorithm based on chaos and interweaving of ranks," *Nonlinear Dyn.*, vol. 84, no. 3, pp. 1595–1607, Jan. 2016.

[77] N. Tsafack, S. Sankar, B. Abd-El-Atty, J. Kengne, J. K. C., A. Belazi, I. Mehmood, A. K. Bashir, O.-Y. Song, and A. A. A. El-Latif, "A new chaotic map with dynamic analysis and encryption application in Internet of health things," *IEEE Access*, vol. 8, pp. 137731–137744, Jul. 2020.

[78] Y.-Q. Zhang and X.-Y. Wang, "A symmetric image encryption algorithm based on mixed linear–nonlinear coupled map lattice," *Inf. Sci.*, vol. 273, pp. 329–351, Jul. 2014.

[79] T. Nestor, N. De Dieu, K. Jacques, E. Yves, A. Iliyasu, and A. Abd El-Latif, "A multidimensional hyperjerk oscillator: Dynamics analysis, analogue and embedded systems implementation, and its application as a cryptosystem," *Sensors*, vol. 20, no. 1, p. 83, Dec. 2019.

[80] A. Belazi, M. Khan, A. A. A. El-Latif, and S. Belghith, "Efficient cryptosystem approaches: S-boxes and permutation–substitution-based encryption," *Nonlinear Dyn.*, vol. 87, no. 1, pp. 337–361, Jan. 2017.

[81] J. S. Teh, M. Alawida, and Y. C. Sii, "Implementation and practical problems of chaos-based cryptography revisited," *J. Inf. Secur. Appl.*, vol. 50, Feb. 2020, Art. no. 102421.

[82] P. S. Sneha, S. Sankar, and A. S. Kumar, "A chaotic colour image encryption scheme combining Walsh–Hadamard transform and Arnold–Tent maps," *J. Ambient Intell. Humanized Comput.*, vol. 11, no. 3, pp. 1289–1308, Mar. 2020.

[83] N. Tsafack, J. Kengne, B. Abd-El-Atty, A. M. Iliyasu, K. Hirota, and A. A. A. EL-Latif, "Design and implementation of a simple dynamical 4-D chaotic circuit with applications in image encryption," *Inf. Sci.*, vol. 515, pp. 191–217, Apr. 2020.

[84] Q. Wang, Q. Guo, L. Lei, and J. Zhou, "Linear exchanging operation and random phase encoding in gyrator transform domain for double image encryption," *Optik*, vol. 124, no. 24, pp. 6707–6712, Dec. 2013.

[85] Z. T. Njitacke, S. D. Isaac, T. Nestor, and J. Kengne, "Window of multistability and its control in a simple 3D hopfield neural network: Application to biomedical image encryption," *Neural Comput. Appl.*, pp. 1–20, Nov. 2020.

[86] A.-V. Diaconu, "Circular inter–intra pixels bit-level permutation and chaos-based image encryption," *Inf. Sci.*, vols. 355–356, pp. 314–327, Aug. 2016.

[87] L. Liu, Q. Zhang, and X. Wei, "A RGB image encryption algorithm based on DNA encoding and chaos map," *Comput. Electr. Eng.*, vol. 38, no. 5, pp. 1240–1248, Sep. 2012.

[88] M. Alawida, J. S. Teh, A. Samsudin, and W. H. Alshoura, "An image encryption scheme based on hybridizing digital chaos and finite state machine," *Signal Process.*, vol. 164, pp. 249–266, Nov. 2019.

[89] Z. Hua, Y. Zhou, C.-M. Pun, and C. P. Chen, "2D sine logistic modulation map for image encryption," *Inf. Sci.*, vol. 297, pp. 80–94, Mar. 2015.

[90] L. Huang, S. Cai, X. Xiong, and M. Xiao, "On symmetric color image encryption system with permutation-diffusion simultaneous operation," *Opt. Lasers Eng.*, vol. 115, pp. 7–20, Apr. 2019.

[91] H. Diab, "An efficient chaotic image cryptosystem based on simultaneous permutation and diffusion operations," *IEEE Access*, vol. 6, pp. 42227–42244, Jul. 2018.

[92] M. Alawida, A. Samsudin, J. S. Teh, and R. S. Alkhawaldeh, "A new hybrid digital chaotic system with applications in image encryption," *Signal Process.*, vol. 160, pp. 45–58, Jul. 2019.

[93] T. Gopalakrishnan and S. Ramakrishnan, "Image encryption using hyperchaotic map for permutation and diffusion by multiple hyper-chaotic maps," *Wireless Pers. Commun.*, vol. 109, no. 1, pp. 437–454, Nov. 2019.

JHARNA TAMANG received the B.Sc. degree from the Darjeeling Government College, under the University of North Bengal, and the M.Sc. degree in mathematics from the Sikkim Manipal Institute of Technology (SMIT), Sikkim Manipal University (SMU), Majitar, India, where she is currently pursuing the Ph.D. degree, under the guidance of Dr. A. Saha, with the Department of Mathematics. She has published more than 12 research articles in the mentioned field with reputed international journals. Her research fields include dynamical systems, bifurcation, chaos, quasiperiodicity, and nonlinear waves in plasmas.

JEAN DE DIEU NKAPKOP received the Ph.D. degree in automatics, electronics, and informatics from the University of Ngaoundéré, Cameroon, in 2017, and in electronic engineering and telecommunications from the Technical University of Cluj-Napoca, Romania, in 2017. He is currently a Lecturer with the Electrical Engineering and Industrial Computing Department, University of Douala, Cameroon. His research interests include cryptography, chaos-based image encryption, and image processing.

MUHAMMAD FAZAL IJAZ received the M.S. and Ph.D. degrees from Dongguk University, Seoul, South Korea. He is currently working as an Assistant Professor with the Department of Intelligent Mechatronics Engineering, Sejong University, Seoul. He is the author of multi-disciplinary articles. His research interests include machine learning, healthcare analytics, supply chain management, big data, and data mining.

PUNAM KUMARI PRASAD received the B.Sc. degree from the Sikkim Government College, Sikkim University, Tadong, India, in 2011, the M.Sc. degree in mathematics from the Sikkim Manipal Institute of Technology (SMIT), Sikkim Manipal University (SMU), India, in 2013, and the B.Ed. degree from the Loyola College of Education, Sikkim University, Namchi, India, in 2015. She is currently pursuing the Ph.D. degree, under the guidance of Dr. A. Saha, with the Department of Mathematics, SMIT, SMU.

She has few research publications regarding the study of nonlinear plasma waves in space and astrophysical environments. Her research fields include dynamical systems, bifurcation, chaos, quasiperiodicity, and nonlinear waves in space and astrophysical plasmas.

NESTOR TSAFACK was born in Santchou, Cameroon, in 1989. He received the B.S. and M.S. degrees in electronics from the University of Dschang, Cameroon, in 2013 and 2016, respectively, and the DIPET II in electrotechnics from the University of Bamenda, in 2016. He is currently pursuing the Ph.D. degree with the University of Dschang, Cameroon, under the guidance of Prof. J. Kengne. He is serving for the Department of Electrical Engineering, Government Technical High School Ekite. He also serves as a reviewer for renowned international journals. His research interests include image processing, nonlinear systems analysis, and engineering application of complex dynamical systems, and he has authored or coauthored many journal articles in the mentioned fields.

ASIT SAHA received the M.Sc. degree (Hons.) from the University of North Bengal, in 2005, where he received the University Medal and the Kiran Chandra Bhattachariya Medal for securing distinction marks, and the Ph.D. degree from Visva-Bharati University, Santiniketan, India, in 2016. He is currently an Assistant Professor (Selection Grade) with the Department of Mathematics, Sikkim Manipal Institute of Technology, Sikkim Manipal University, Majitar, India. He is currently serving as an Editor for a reputed Q1 international interdisciplinary journal "*The European Physical Journal Plus (EPJ Plus).*" He has published more than 80 research articles with reputed international journals. His research areas include bifurcation, chaotic, and multistability behaviors of nonlinear waves in plasmas. He was the first person to apply the theory of planar dynamical systems in the area of plasma waves. His other interest is to employ the concept of nonlinear dynamics in different areas of physical problems.

JACQUES KENGNE was born in Bamougoum, Cameroon, in 1971. He received the M.Sc. and Ph.D. degrees in electronics from the Faculty of Sciences, University of Dschang, in 2007 and 2011, respectively. From 2010 to 2012, he worked as a Lecturer with the Department of Electrical Engineering, IUT-FV, University of Dschang, where he served as a Senior Lecturer from 2012 to 2016. In 2016, he was appointed to an Associate Professor with the University of Dschang. He has authored or coauthored more than 60 journal articles. His research interests include nonlinear systems and circuits, chaos, multistability, and chaos synchronization with applications. He also serves as a Reviewer for renowned international journals, including *IJBC, Communications in Nonlinear Science and Numerical Simulation*, *International Journal of Dynamics and Control*, *Nonlinear Dynamics*, *Chaos, Solitons & Fractals*, and IEEE Transactions on Circuits and Systems I: Regular Papers.

YOUNGDOO SON received the Ph.D. degree from Seoul National University, in 2015. From 2015 to 2017, he was a Visiting Research Scholar and Postdoctoral Fellow with Rutgers, The State University of New Jersey and Seoul National University, respectively. Since 2017, he has been working as an Assistant Professor with the Department of Industrial and Systems Engineering, Dongguk University, South Korea. He is specialized in data science, machine learning methods, and their applications to industrial, business, and financial problems. His research interests include machine learning methods and applications to industry problems.

• • •